Published July 6, 2015



# p53 protects against genome instability following centriole duplication failure

Bramwell G. Lambrus,[1] Yumi Uetake,[2] Kevin M. Clutario,[1] Vikas Daggubati,[1] Michael Snyder,[1] Greenfield Sluder,[2] and Andrew J. Holland[1]

[1]Department of Molecular Biology and Genetics, Johns Hopkins University School of Medicine, Baltimore, MD 21205
[2]Department of Cell and Developmental Biology, University of Massachusetts Medical School, Worcester, MA 01655

Centriole function has been difficult to study because of a lack of specific tools that allow persistent and reversible centriole depletion. Here we combined gene targeting with an auxin-inducible degradation system to achieve rapid, titratable, and reversible control of Polo-like kinase 4 (Plk4), a master regulator of centriole biogenesis. Depletion of Plk4 led to a failure of centriole duplication that produced an irreversible cell cycle arrest within a few divisions. This arrest was not a result of a prolonged mitosis, chromosome segregation errors, or cytokinesis failure. Depleting p53 allowed cells that fail centriole duplication to proliferate indefinitely. Washout of auxin and restoration of endogenous Plk4 levels in cells that lack centrioles led to the penetrant formation of de novo centrioles that gained the ability to organize microtubules and duplicate. In summary, we uncover a p53-dependent surveillance mechanism that protects against genome instability by preventing cell growth after centriole duplication failure.

## Introduction

Centrosomes are the main microtubule-organizing centers (MTOCs) of most animal cells and are composed of a pair of centrioles surrounded by pericentriolar material (PCM; Nigg and Raff, 2009; Gönczy, 2012). Centrioles act as the centrosome organizer and thus their duplication controls centrosome number. Like DNA, centrioles duplicate exactly once per cell cycle, with a single new procentriole forming on the wall of each existing centriole (Tsou and Stearns, 2006). This tightly controlled process ensures the generation of two centrosomes to form the poles of the bipolar mitotic spindle. Errors in centriole duplication lead to abnormal centrosome number, which can result in chromosome segregation errors and the production of aneuploid progeny (Ganem et al., 2009; Silkworth et al., 2009). Aberrations in centrosome number have been associated with several human diseases, including cancer and neurodevelopmental disorders (Nigg and Raff, 2009).

Canonical centriole duplication begins at the G1/S transition with the assembly of a single cartwheel structure on the wall of each preexisting mother centriole. The cartwheel then templates the formation of a procentriole by providing a scaffold onto which microtubules are loaded (Kitagawa et al., 2011; van Breugel et al., 2011, 2014). In addition to this canonical pathway of centriole assembly, de novo centriole formation can occur in the absence of existing centrioles (Miki-Noumura, 1977; Szöllosi and Ozil, 1991; Palazzo et al., 1992; Marshall et al., 2001; Suh et al., 2002). A striking example of this process occurs in mouse embryos, where cell divisions continue in the absence of centrioles until the 64-cell stage, at which point centrioles are created de novo (Szollosi et al., 1972). In vertebrate somatic cells, a variable number of de novo centrioles are generated after experimental removal of existing centrioles (Khodjakov et al., 2002; La Terra et al., 2005; Uetake et al., 2007). It is therefore thought that existing centrioles act to suppress de novo centriole assembly, although the molecular mechanism for this suppression remains unclear.

Previous approaches to study the immediate consequence of centriole loss in human cells have relied on laser ablation or microsurgery (Khodjakov et al., 2002; La Terra et al., 2005; Uetake et al., 2007). These elegant approaches only transiently remove centrioles from a small number of cells. Permanent centriole loss has been achieved through the knockout of essential centriole components (Sir et al., 2013; Bazzi and Anderson, 2014; Izquierdo et al., 2014). Although informative, these studies did not address the immediate effects of centriole duplication failure and were unable to temporally control formation of new centrioles.

Polo-like kinase 4 (Plk4) has emerged as a conserved, dose-dependent regulator of centriole copy number and offers an attractive target to reversibly modulate centriole number in populations of cells (Bettencourt-Dias et al., 2005; Habedanck et al., 2005). Plk4 is a self-regulating enzyme that phosphorylates itself to promote its own destruction (Cunha-Ferreira et

Correspondence to Andrew J. Holland: aholland@jhmi.edu

Abbreviations used in this paper: AAV, adeno-associated virus; AID, auxin-inducible degron; IAA, indole-3-acetic acid; MTOC, microtubule-organizing center; PCM, pericentriolar material; Plk4, Polo-like kinase 4.



Supplemental Material can be found at:
http://jcb.rupress.org/content/suppl/2015/07/06/jcb.201502089.DC1.html

The Rockefeller University Press $30.00
J. Cell Biol. Vol. 210 No. 1 63–77
www.jcb.org/cgi/doi/10.1083/jcb.201502089

Published July 6, 2015

al., 2009, 2013; Rogers et al., 2009; Guderian et al., 2010; Holland et al., 2010; Brownlee et al., 2011; Klebba et al., 2013). This autoregulated destruction plays an important role in controlling the abundance of endogenous Plk4 and thereby helps to limit centriole duplication to once per cell cycle (Holland et al., 2012b). RNA interference and knock-in approaches have been used to inhibit Plk4 function, but these strategies are slow acting and are not readily reversible. Inhibition of Plk4 kinase activity offers a powerful alternative to manipulate Plk4 function. However, specific kinase inhibitors are difficult to develop (Holland and Cleveland, 2014; Mason et al., 2014). In addition, inhibiting Plk4 activity greatly increases protein abundance, making it challenging to dissect the relative contribution of loss of kinase activity and increased protein abundance (Holland et al., 2010).

In this study, we developed a chemical genetics approach to rapidly and reversibly control Plk4 protein abundance in cells. Manipulating endogenous Plk4 levels allowed the reversible depletion of centrioles from populations of cycling cells and uncovered the existence of a p53-dependent pathway that guards against genome instability by preventing cellular proliferation after centriole duplication failure. By taking advantage of the acute and titratable depletion of Plk4, our data define the threshold level of Plk4 required for centriole assembly and establish the consequence of acute Plk4 depletion on centriole composition.

## Results

### A novel system for rapidly and reversibly controlling Plk4 levels

To study the immediate effects caused by Plk4 depletion, we turned to an auxin-inducible degradation system that allows for posttranslational control of protein abundance with the plant hormone auxin (Nishimura et al., 2009). In plants, auxin promotes the binding of the F-box protein osTIR1 to proteins containing an auxin-inducible degron (AID). In the presence of auxin, osTIR1 recruits AID-containing substrates to the Skp1, Cullin, and F-Box ubiquitin ligase, which ubiquitinates the AID-containing protein and targets it for proteasomal degradation. Ectopic expression of osTIR1 in mammalian cells generates an $SCF^{TIR1}$ complex and enables auxin-inducible destruction of AID-tagged transgenes (Holland et al., 2012a), suggesting that the AID system could also be applied to posttranslationally regulate the stability and abundance of endogenous Plk4.

We used sequential rounds of gene targeting to knock-in the AID onto the C terminus of both endogenous Plk4 alleles in nontransformed, telomerase-immortalized, human RPE-1 cells (Fig. S1, A and B). To facilitate detection, each $Plk4^{AID}$ allele was tagged at the C terminus with a HA or 3× FLAG tag. Two $Plk4^{AID\text{-}HA/AID\text{-}3xFLAG}$ (hereafter referred to as $Plk4^{AID/AID}$) clones were obtained and behaved similarly in all assays. $Plk4^{AID/AID}$ cells exhibited normal centrosome copy number and cell cycle profiles (Fig. S1, C and D), and both $Plk4^{AID\text{-}HA}$ and $Plk4^{AID\text{-}FLAG}$ localized to the centrioles of cells in interphase and mitosis in a manner that was indistinguishable from wild-type Plk4 (Fig. S1 E). We conclude that $Plk4^{AID}$ is capable of supporting Plk4 function in centriole duplication.

We stably expressed osTIR1-9xMyc in $Plk4^{AID/AID}$ cells to place the stability of endogenous $Plk4^{AID}$ under the control of exogenous auxin (Fig. 1 A). To analyze Plk4 protein levels, we immunoprecipitated $Plk4^{AID\text{-}3xFLAG}$ from cell lysates using a FLAG antibody and determined the abundance of Plk4 by immunoblot. Addition of the auxin indole-3-acetic acid (IAA) to $Plk4^{AID/AID}$ cells led to rapid Plk4 degradation, with Plk4 falling below the limit of detection within 10 min of IAA addition (Fig. 1 B). The level of Plk4 at the centrosome was measured at various times after IAA addition using antibodies raised to the FLAG tag or to the C terminus of Plk4. Staining with the monoclonal FLAG antibody revealed that the level of Plk4 at the centrosomes of interphase cells declined by >95% within 30 min of IAA addition (Fig. 1, C and D), whereas staining with a polyclonal antibody to the C terminus of Plk4 revealed a >80% reduction during the same time period (Fig. S1 F). Plk4 destruction occurred in all cell cycle phases (Fig. 1 E) and required the presence of the osTIR1 F-box protein (Fig. S1 G). Importantly, the degradation of Plk4 was fully reversible, with the level of Plk4 at the centriole recovering to original levels within 3 h of IAA removal (Fig. 1 F).

To examine whether treatment with IAA leads to the expected failure of centriole duplication, we assessed centriole number in cells undergoing mitosis one cell cycle (30 h) after IAA addition. In untreated $Plk4^{AID/AID}$ cells, centriole duplication occurred successfully in >90% of cells (0 µM IAA; Fig. 2, A and B). In contrast, IAA addition caused a failure of centriole duplication in >90% of $Plk4^{AID/AID}$ cells (500 µM IAA; Fig. 2, A and B). We conclude that $Plk4^{AID/AID}$ cells offer a new tool to achieve rapid and reversible depletion of endogenous Plk4.

### A graded reduction in protein levels reveals a threshold level of Plk4 required for centriole duplication

Reduced expression of Plk4 has been associated with tumorigenesis, but it remains unknown how much Plk4 protein is required for centriole duplication (Ko et al., 2005; Pellegrino et al., 2010; Liu et al., 2012). Because Plk4 autoregulates its own stability, generating a progressive reduction in Plk4 protein levels is challenging, as a reduced abundance of Plk4 mRNA may not lead to a comparable down-regulation of Plk4 protein (Holland et al., 2012a). We therefore set out to use auxin-inducible destruction to generate a graded reduction in Plk4 levels. We used quantitative microscopy with directly labeled Plk4 primary antibodies to determine the abundance of Plk4 at the centriole in cells treated with various concentrations of IAA. Exposing $Plk4^{AID/AID}$ cells to increasing concentrations of IAA resulted in gradual reduction in the average level of Plk4 at the centriole (Fig. 2 A). We examined whether centriole duplication occurred successfully with different levels of Plk4 protein. In cells treated with 1 µM IAA, the average level of Plk4 at the centrosome was 81% of that in untreated cells (Fig. 2, A and B). Under these conditions, centrioles duplicated in >75% of cells. However, at 10 µM IAA, whereas centrosomal Plk4 levels were maintained at 57% of that in control cells, <10% of cells underwent centriole duplication (Fig. 2, A and B). We conclude that Plk4 levels are finely balanced and that a less than twofold reduction in the level of Plk4 at the centrosome leads to a failure of centriole duplication.

### The centriole localization of STIL is uniquely sensitive to the levels of Plk4

RNA interference of Plk4 leads to slow protein depletion, making it challenging to distinguish between direct and indirect effects of Plk4 removal. The ability to rapidly remove Plk4 from cells provided an opportunity to identify proteins that directly

Published July 6, 2015

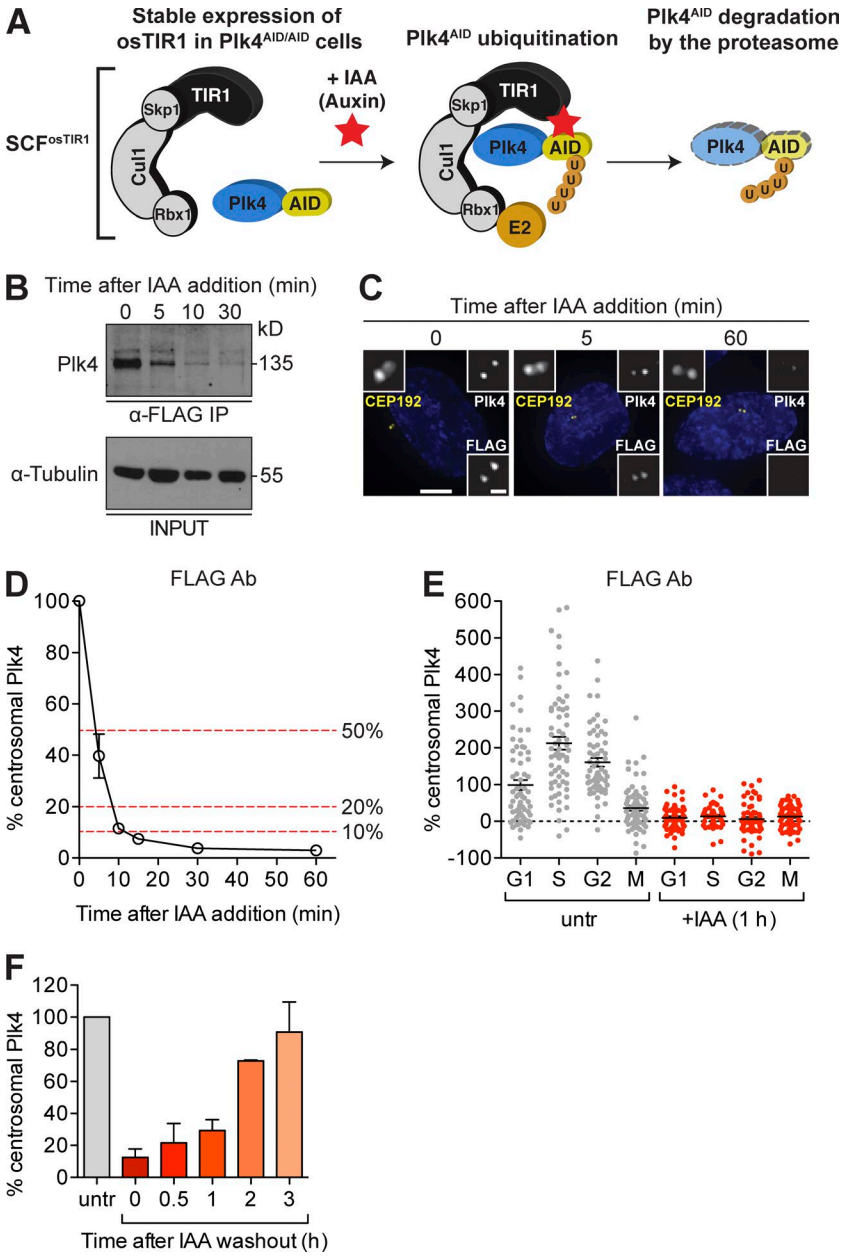


Figure 1. **Inducible destruction of endogenous Plk4.** (A) Schematic outlining the strategy for the auxin-inducible destruction of Plk4. (B) Western blot showing the levels of immunoprecipitated Plk4-AID-FLAG at the indicated times after IAA addition. (C) Plk4$^{AID/AID}$ cells immunostained for CEP192, Plk4, and FLAG after treatment with IAA for the indicated time. Bars: (main) 5 µm; (inset) 1 µm. (D) Quantification of the level of FLAG-tagged Plk4-AID at the centrosome at the indicated times after IAA addition. Each condition represents the mean of >70 cells from at least two independent experiments. (E) Quantification of the level of FLAG-tagged Plk4-AID at the centrosome at the indicated cell cycle stages. Horizontal line represents the mean of >70 cells from two independent experiments. (F) Quantification of Plk4 protein levels at the centrosome at the indicated time after IAA washout. Plk4 levels return to normal within 3 h of auxin removal. Each bar represents the mean of >70 cells from at least two independent experiments. All error bars in the figure represent the SEM.

depend on Plk4 for recruitment to the centriole. We used immunofluorescence microscopy to examine the abundance of 10 proteins (CPAP, CEP135, CEP152, CEP192, SAS6, CNAP1, CEP164, Centrin, γ-tubulin, and STIL) at the centrosome 1 h after Plk4 destruction with IAA. Because the abundance of several centriole proteins are reduced after mitosis (Strnad et al., 2007; Tang et al., 2009; Tang et al., 2011; Arquint et al., 2012; Arquint and Nigg, 2014), our measurements were made in S/G2 cells that were marked by the presence of CENP-F (Hussein and Taylor, 2002). Of the 10 proteins examined, the localization of STIL was uniquely sensitive to a reduction in Plk4 levels: the abundance of STIL at the centriole was reduced by >75% 1 h after IAA addition, whereas total protein levels remained unchanged (Fig. 2 C). These data are consistent with a recent study showing that Plk4 binds to STIL (Ohta et al., 2014). STIL has been proposed to recruit SAS6 to the centriole through a direct, phosphorylation-dependent interaction (Dzhindzhev et al., 2014; Ohta et al., 2014). However, whereas STIL levels declined dramatically by 1 h after acute Plk4 destruction, we observed only a modest change in centriole SAS6 levels, suggesting STIL is not required to maintain existing SAS6 at the centriole (Fig. 2 C).

## Cells lacking Plk4 undergo a cell cycle arrest

We next examined the chronic effect of Plk4 depletion in RPE1 cells. Although Plk4$^{+/+}$ cells proliferated normally in the presence of IAA, addition of IAA to Plk4$^{AID/AID}$ cells resulted in a cell cycle arrest 48 h after treatment began (Fig. 3 A). Interphase Plk4$^{AID/AID}$ cells exhibited a dramatic reduction in centriole number by 24 h after IAA addition (Fig. 3 B). Centriole number decreased further by 48 h after Plk4 degradation, giving rise to 22% of cells that lack centrioles. After this time, centriole content changed only slowly, consistent with the fact that the vast majority of cells cease proliferating by 48 h after IAA addition.

To evaluate the long-term growth potential of cells that lack endogenous Plk4, we performed clonogenic survival as-

Published July 6, 2015

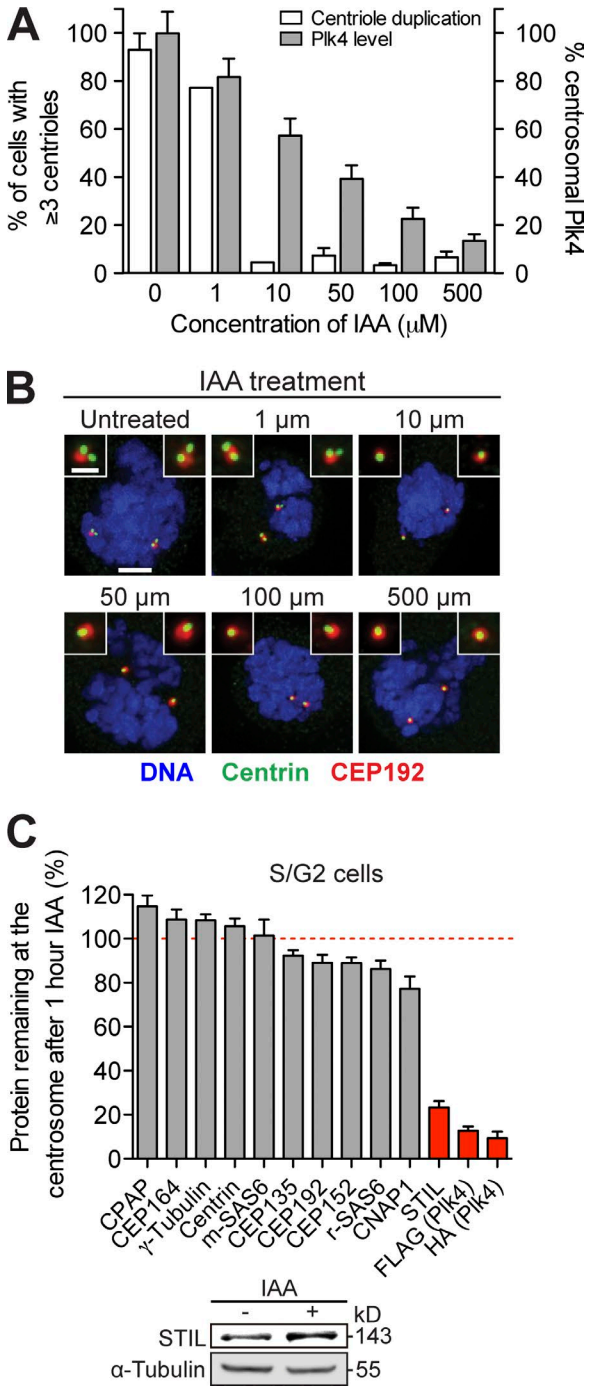


Figure 2. **The centriole localization of STIL requires Plk4.** (A) Quantification of Plk4 protein levels at the centrosome of interphase cells at 24 h after addition of the indicated concentrations of IAA (gray bars). The fraction of mitotic cells that underwent successful centriole duplication (three or more centrioles) was quantified in the same samples (open bars). Bars represent the mean of >40 cells from two independent experiments. (B) Representative images of Plk4$^{AID/AID}$ cells immunostained with CEP192 and Centrin after treatment with the indicated dose of IAA for 24 h. Bars: (main) 5 μm; (inset) 1 μm. (C) Quantification of relative protein abundance at the centrosome of S or G2 phase (CENP-F positive) cells 1 h after IAA addition. Centriole recruitment of STIL requires Plk4. r-SAS6, rabbit SAS6 antibody; m-SAS6, mouse SAS6 antibody. Bars represent the mean of >35 cells from two independent experiments. Immunoblot shows no change in the level of endogenous STIL after Plk4 degradation. All error bars in the figure represent the SEM.

says. IAA addition prevented colony formation in Plk4$^{AID/AID}$ cells, but only modestly affected the survival of Plk4$^{+/+}$ and Plk4$^{+/AID}$ cells (Fig. S2, A and B). To determine whether Plk4 depletion leads to an irreversible cell cycle arrest, we treated Plk4$^{AID/AID}$ cells with IAA for either 1 h or 4 d and then restored Plk4 levels by washing out IAA. Although 1 h of IAA treatment had no affect on cell growth, washout of IAA after 4 d of treatment was unable to restore cell proliferation (Fig. 3 C). We conclude that chronic depletion of Plk4 leads to an irreversible cell cycle arrest.

To examine the effect of centriole loss on cell division, we created Plk4$^{AID/AID}$ cells coexpressing TagRFP-tubulin, EGFP-Histone H2B, and EGFP-Cep63 (to mark parental centrioles; Sir et al., 2011) and monitored cells by time-lapse microscopy. Untreated control cells progressed though mitosis with a mean time of 44 min and contained a single EGFP-Cep63 focus at each spindle pole (Fig. 3, D and G; and Video 1). In the first 24 h after Plk4 destruction, all cells formed bipolar spindles and divided normally, albeit with a modest mitotic delay (mean time of 58 min to divide; Fig. 3, D and E). However, by the second day after IAA addition the duration of mitosis increased to a mean time of 84 min (Fig. 3 D). Nevertheless, all cells progressed to anaphase and successfully executed cytokinesis (Fig. 3 E). Although there was an increase in chromosome segregation errors in auxin-treated cells, the frequency of these errors was too small to account for the growth arrest (Fig. 3 E). Interestingly, in a significant fraction of divisions, multi-lobed nuclei formed after apparently normal anaphase chromosome movements (Fig. 3, F and G; and Video 2). Importantly, these cell division defects were not caused by drug treatment alone, as IAA had little effect on mitotic timing or nuclear shape in Plk4$^{+/+}$ RPE1 cells (Fig. S2, C and D).

### The cell cycle arrest after centriole duplication failure is not caused by a prolonged mitosis

Using fixed imaging, we examined the number of centrioles at various time points after IAA treatment. As expected, untreated control cells divided with two centrioles at each spindle pole (Fig. 4, A and B). In contrast, at 1 d after IAA addition, >90% of Plk4$^{AID/AID}$ cells divided with a single centriole at each spindle pole, whereas at days 2 and 3 after IAA addition >65% of cells divided with an asymmetric spindle comprised of an acentriolar pole and a pole containing a single centriole (Fig. 4, A and B). Cell divisions were rarely observed to take place in the absence of centrioles.

Previous work has shown that prolonging prometaphase to >90 min leads to a durable G1 arrest in RPE1 cells (Uetake and Sluder, 2010). We therefore investigated whether an increased mitotic duration could account for the cell cycle arrest observed after centriole duplication failure. We first set out to determine the window of tolerance for prometaphase duration in Plk4$^{AID/AID}$ cells. Plk4$^{AID/AID}$ cells were treated with 0.08 μM nocodazole for 6 h and the proliferative fate of daughter cells was monitored using time-lapse microscopy. Similar to the parental RPE1 cells, prolonging the duration of prometaphase in Plk4$^{AID/AID}$ cells to >97 min caused a cell cycle arrest in all resulting daughters (Fig. S3 A). Addition of IAA to parental RPE1 cells shortened the window of prometaphase tolerance to 60 min (Fig. S3 B). Consequently, we considered 60 min to be the prometaphase threshold for IAA-treated cells.

Published July 6, 2015

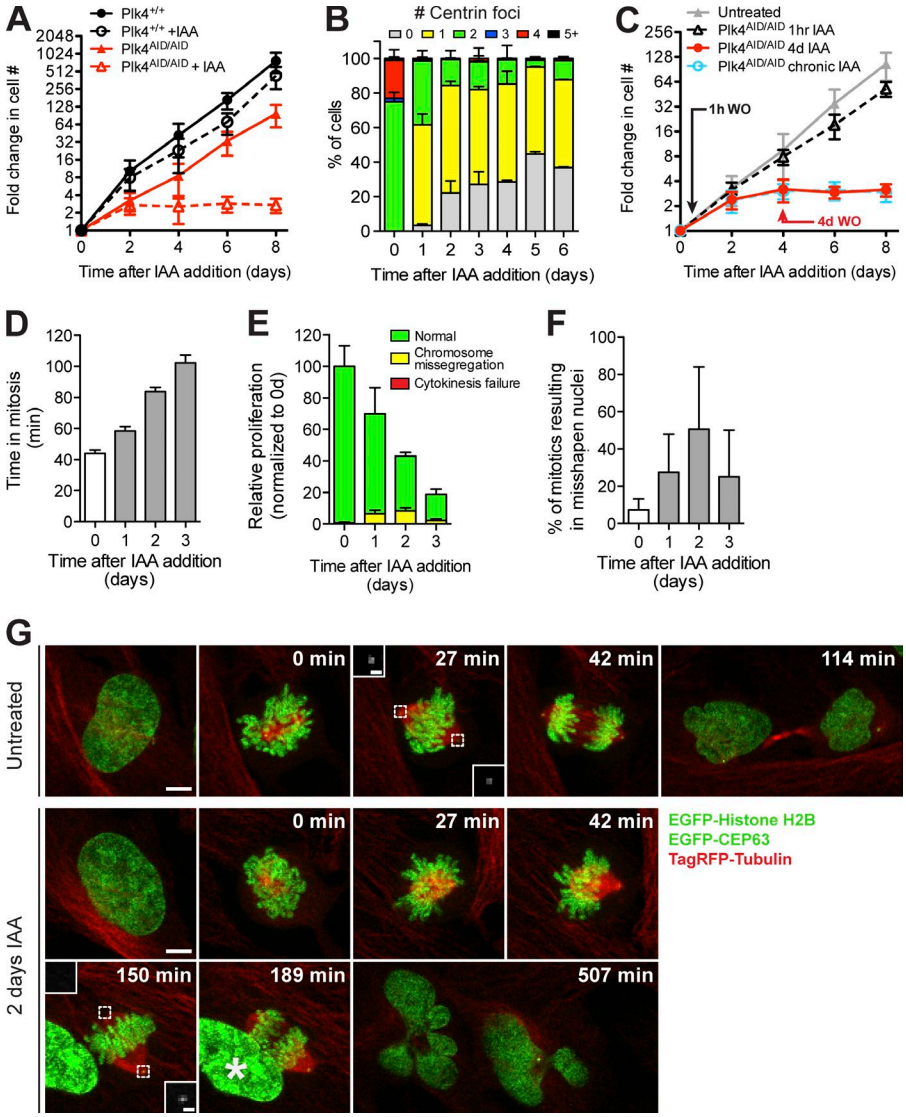


Figure 3. **Plk4 depletion leads to a failure of centriole duplication followed by a cell cycle arrest.** (A) Graph showing the fold increase in cell number after IAA addition. Plk4 destruction leads to a cell cycle arrest in Plk4$^{AID/AID}$ cells. Points show the mean of at least two independent experiments performed in triplicate. (B) Quantification of the number of Centrin foci per cell in interphase at indicated times after IAA addition. Bars represent the mean of >100 cells from two independent experiments. (C) Graph showing the fold increase in cell number after IAA washout (WO) and restoration of Plk4 levels. Centriole loss leads to an irreversible cell cycle arrest. Points show the mean of at least two independent experiments performed in triplicate. (D) Quantification of the duration of mitosis. Measurements were taken over a 24-h period at indicated times after IAA addition. Bars represent the mean of >60 cells from two independent experiments. (E) Quantification of relative cell proliferation and fraction of cells undergoing chromosome missegregation or cytokinesis failure. Measurements were taken over a 24-h period at indicated times after IAA addition. Bars represent the mean of >40 cells from two independent experiments. (F) Quantification of the frequency of divisions resulting in the formation of misshapen nuclei. Measurements were taken over a 24-h period at indicated times after IAA addition. Bars represent the mean of >40 cells from two independent experiments. All error bars in the figure represent the SEM. (G) Selected images from a time-lapse series of untreated or IAA-treated Plk4$^{AID/AID}$ cells coexpressing histone TagRFP-tubulin, EGFP-Histone H2B, and EGFP-CEP63. Insets show EGFP-CEP63 at the centrosome. Time is indicated in minutes relative to nuclear envelope breakdown (time point 0). Note that the cell treated with IAA for 2 d exhibits an asymmetric spindle with one acentriolar pole. The interphase nucleus (asterisk) at 189 min later left the field of view. Bars: (main) 5 µm; (inset) 1 µm.

We next traced the lineage of individual Plk4$^{AID/AID}$ cells treated with IAA (Fig. S3 C). Only cells that entered the first division within 6 h of IAA addition were considered in our analysis. As a consequence, the first mitosis nearly always occurred with two centrioles at each spindle pole and all daughter cells continued to proliferate (Fig. 4, B and C). In subsequent divisions, centriole number was successively reduced as expected from failed centriole duplication and continued cell growth. 48% of daughter cells arrested after the second mitosis, whereas 78% of daughters arrested after the third mitosis and all daughter cells arrested after the fourth mitosis (Fig. 4 C). The delayed growth arrest after Plk4 destruction strongly suggests that a stress associated with a failure of centriole duplication not loss of Plk4, per se, is responsible for the proliferative arrest.

In the second division after Plk4 destruction, nearly all daughters of mothers that spent >60 min in prometaphase arrested as expected (Fig. 4 D). However, 37% of the daughters of mothers that spent <60 min in prometaphase also arrested and this fraction increased to 52% and 100% in the third and fourth divisions, respectively. It was previously shown that continuous inhibition of p38 MAPK activity with the small molecule SB203580 overcame the proliferative block caused by a prolonged prometaphase induced by transient nocodazole treatment. However, inhibition of p38 MAPK activity did not prevent or delay the cell cycle arrest caused by Plk4 loss (Fig. S3 D). We conclude that the cell cycle arrest caused by centriole duplication failure is not simply a result of a prolonged prometaphase duration (Uetake and Sluder, 2010).

Previous work has shown that DNA damage, Hippo pathway activation, or excessive oxidative stress can cause cell cycle arrest (Ganem et al., 2014). However, addition of IAA for 3 d did not lead to a detectable increase in DNA damage (measured by γH2A.X phosphorylation) or Hippo pathway activation (revealed by LATS2 or YAP phosphorylation) in Plk4$^{AID/AID}$ cells (Fig. 4 E). In addition, culturing Plk4$^{AID/AID}$ cells in 3% $O_2$, rather than 21% $O_2$, did not prevent the proliferative arrest after Plk4 destruction (Fig. 4 F). Collectively, our data suggest that DNA damage, Hippo pathway activation, and oxidative stress are unlikely to be the cause of the cell cycle arrest that occurs after a failure of centriole duplication.

## Repression of p53 allows Plk4-depleted cells to proliferate and become acentriolar

RPE1 cells maintain a normal p53 response. Plk4$^{AID/AID}$ cells but not Plk4$^{+/+}$ cells showed stabilization of p53 at 2 and 3 d after IAA addition (Fig. S4 A). We therefore tested whether

Published July 6, 2015

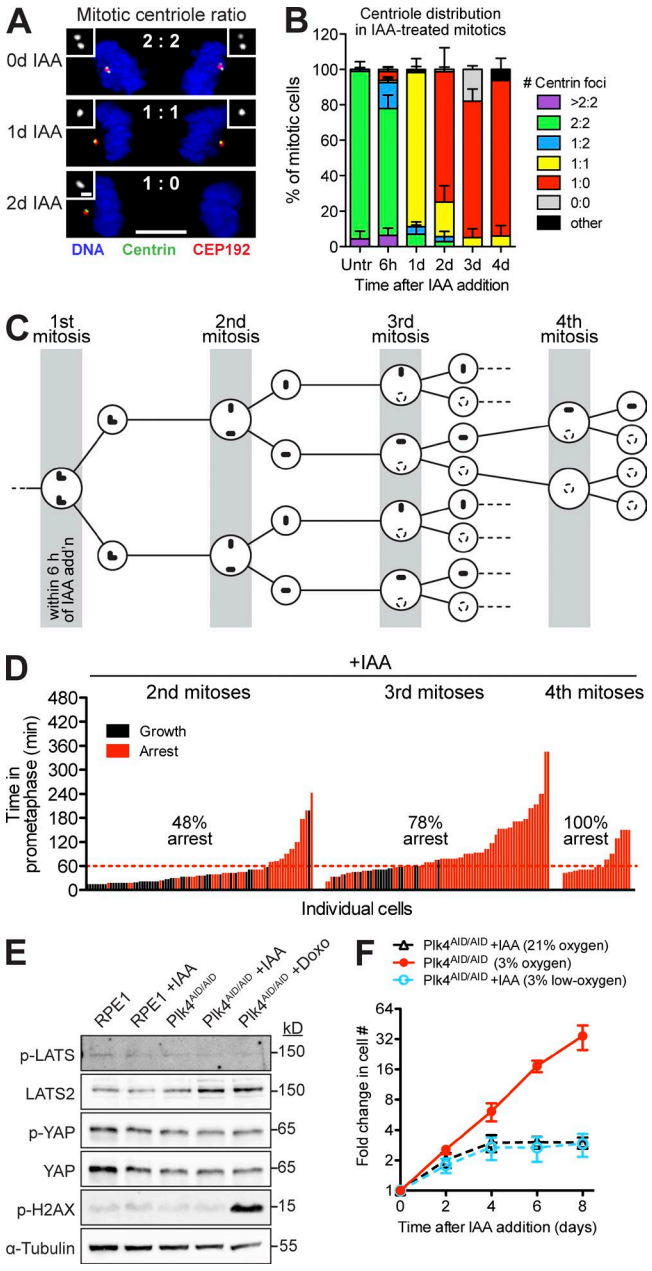


Figure 4. **The IAA-induced cell cycle arrest is not caused by a prolonged mitosis.** (A) Representative images of anaphase cells at indicated times after IAA addition. Cells were costained with Centrin and CEP192. Bars: (main) 5 µm; (inset) 0.5 µm. (B) Quantification of the percentage of cell divisions occurring with the indicated number of centrioles at each spindle pole. Measurements were obtained from fixed samples at the indicated times after IAA addition. Bars represent the mean of >60 cells from two independent experiments. (C) Schematic showing the expected dynamics of centriole dilution after IAA treatment. Cells that undergo mitosis within 6 h of IAA addition almost always contain four centrioles, which dilute out as shown in subsequent divisions. (D) Graph showing the prometaphase duration and proliferative capacity of IAA-treated Plk4$^{AID/AID}$ cells. Each bar represents a daughter cell, its height represents the prometaphase duration of the mother cell, and its color represents the fate of the daughter. Only cells that underwent their first mitosis within 6 h of IAA treatment were analyzed. The dashed red line indicates the maximum time that IAA-treated cells spend in prometaphase before undergoing a cell cycle arrest (Fig. S3 D). Data are taken from two independent experiments ($n$ = 199 prometaphases). (E) Immunoblot showing the levels of phosphorylated LATS, YAP, and Histone H2AX in IAA-treated Plk4$^{AID/AID}$ and parental RPE1 cells. Doxorubicin treatment was used as a control to induce DNA damage. (F) Graph showing the fold increase in cell number in IAA-treated Plk4$^{AID/AID}$ cells grown in normal (21%) or low (3%) oxygen conditions. Points show the mean of two independent experiments performed in triplicate. All error bars in the figure represent the SEM.

stabilization of p53 contributes to the irreversible cell cycle arrest that occurs after Plk4 depletion and centriole duplication failure. Preventing p53 accumulation using a stably expressed p53 shRNA (Fig. S4 B) allowed the continued growth of cells lacking Plk4 (Fig. 5 A) and led to a partial recovery of the clonogenic survival of this population (Fig. S4, C and D). Our findings indicate that a failure of centriole duplication increases p53 levels, eliciting a p53-dependent cell cycle arrest. This is consistent with prior work showing that knockout cells lacking proteins essential for centriole duplication also fail to proliferate in the presence of p53 (Bazzi and Anderson, 2014; Izquierdo et al., 2014).

Plk4$^{AID/AID}$;p53 shRNA cells proliferated indefinitely in the absence of Plk4, and by 6 d after IAA addition Centrin foci were undetectable in >90% of cells (Fig. 5, B and C). To confirm that chronically treated Plk4$^{AID/AID}$;p53 shRNA cells lacked centrioles, we performed immunostaining for a variety of centriole components (CPAP, SAS6, STIL, CEP135, CEP152, and CEP192), but failed to observe centriole foci in the vast majority of cells (unpublished data). We therefore used thin-section EM to evaluate the presence of centrioles. Whereas centrioles were identified in 37/138 transverse sections of control cells, we never observed centrioles in 320 sections from chronically IAA-treated cells. Thus, the failure to detect Centrin foci almost certainly reflects an absence of centrioles in the vast majority of chronically treated Plk4$^{AID/AID}$;p53 shRNA cells (hereafter referred to as acentriolar cells). Consistent with a lack of centrioles, the PCM component γ-tubulin was diffusely localized throughout the cytosol of interphase cells lacking centrioles and failed to concentrate at acentriolar spindle poles (Fig. 5 C). However, 55% of interphase acentriolar cells contained a single focus of the PCM component Pericentrin, suggesting that Pericentrin may have the capacity to self-organize in the absence of centrioles (Fig. S4 E).

To directly examine the divisions of cells lacking centrioles, acentriolar cells coexpressing TagRFP-tubulin, EGFP-Histone H2B, and EGFP-Cep63 were monitored by time-lapse microscopy. Untreated Plk4$^{AID/AID}$;p53 shRNA cells entered mitosis with two microtubule asters and assembled robust bipolar spindles (Fig. 5 E and Video 3). In contrast, in acentriolar cells, microtubule nucleation occurred around the chromatin, before self-organizing into a bipolar spindle with Pericentrin, but not γ-tubulin, concentrated at the poles (Fig. 5, C and E; Video 4; and Fig. S4 E). Acentriolar divisions exhibited an increased mitotic duration (mean of 147 min, compared with 42 min for untreated cells) and were associated with a higher frequency of chromosome segregation errors (40% in acentriolar cells vs. 17% in control cells) and cytokinesis failure (22% in acentriolar cells vs. 1% in control cells) compared with untreated control Plk4$^{AID/AID}$;p53 shRNA cells (Fig. 5 D). Consistent with the increased incidence of cytokinesis failure, a subpopulation of acentriolar cells contained a tetraploid DNA content (Fig. S4 F). These mitotic errors are likely to be the cause of the reduced growth rate and increased doubling time of acentriolar cells (Fig. 5 A and Fig. S4 G). These data are in agreement with the view that centrioles are not strictly essential for mitosis in vertebrate cells, but increase the fidelity of chromosome segre-

Published July 6, 2015

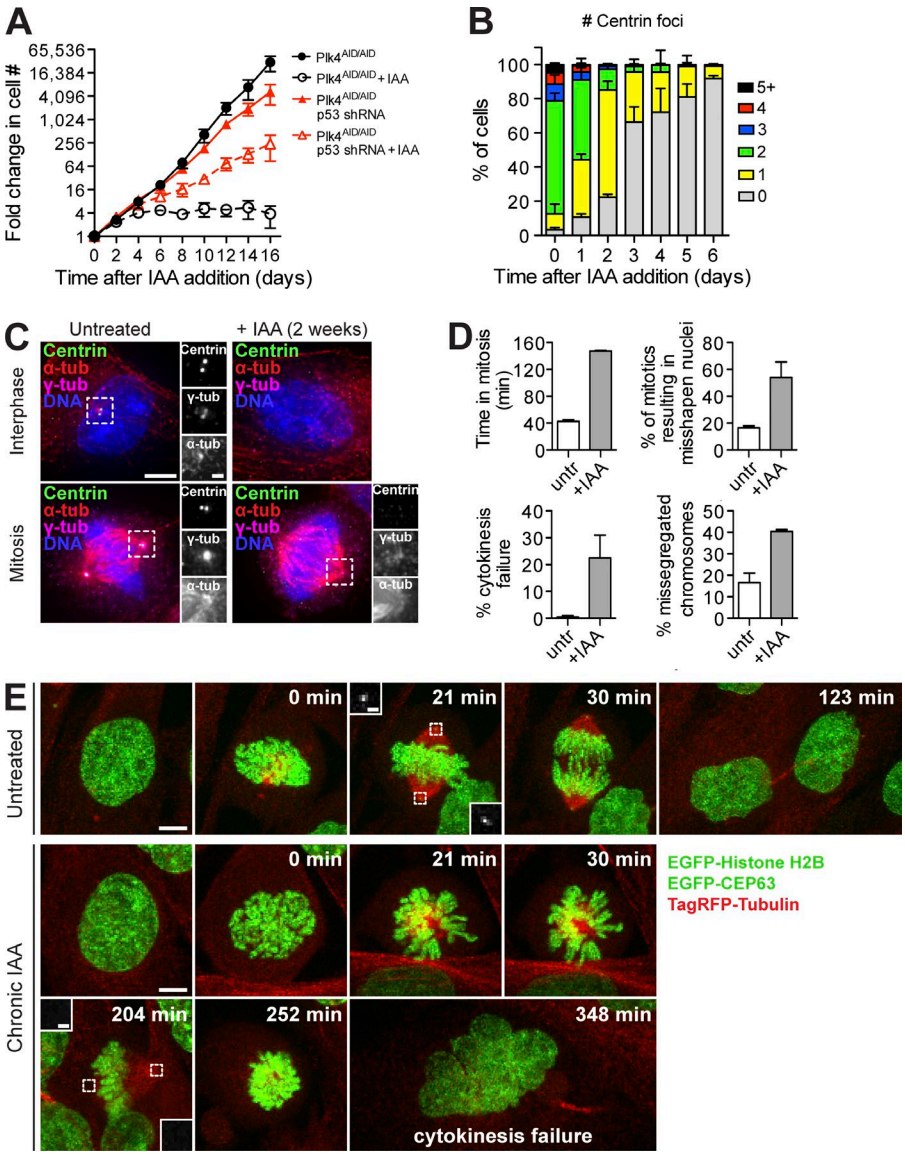


Figure 5. **Depletion of p53 allows continued growth in the absence of Plk4.** (A) Graph showing the fold increase in cell number after IAA addition. Points show the mean of at least two independent experiments performed in triplicate. (B) Quantification of the number of Centrin foci per cell in interphase at indicated times after IAA addition. Bars represent the mean of >150 cells from two independent experiments. (C) Selected images of untreated control or acentriolar Plk4$^{AID/AID}$;p53 shRNA cells immunostained with α-tubulin, γ-tubulin, and Centrin. Bars: (main) 5 µm; (inset) 1 µm. (D) Quantification of the duration of mitosis, the frequency of divisions resulting in the formation of misshapen nuclei, and the frequency of cytokinesis failure and chromosome missegregation in acentriolar Plk4$^{AID/AID}$;p53 shRNA cells. Bars represent the mean of >100 cells from two independent experiments. All error bars in the figure represent the SEM. (E) Selected images from a time-lapse series of untreated control or acentriolar Plk4$^{AID/AID}$;p53 shRNA cells coexpressing histone TagRFP-tubulin, EGFP-Histone H2B, and EGFP-CEP63. Insets show EGFP-CEP63 at the centrosome. The acentriolar cell spends longer in mitosis and fails cytokinesis. Time is indicated in minutes relative to nuclear envelope breakdown (time point 0). Bars: (main) 5 µm; (inset) 1 µm.

gation and cytokinesis (Khodjakov and Rieder, 2001; Debec et al., 2010; Sir et al., 2013).

### Restoration of endogenous Plk4 levels in acentriolar cells results in de novo centriole formation

In vertebrate somatic cells, de novo centriole assembly is initiated after the eradication of the existing centrioles by laser ablation or microsurgery (Khodjakov et al., 2002; La Terra et al., 2005; Uetake et al., 2007). In this case a variable number of de novo centrioles are spontaneously generated. We therefore examined the effect of restoring endogenous Plk4 levels in acentriolar cells. Endogenous Plk4 levels returned to normal within 12 h of IAA washout (Fig. 6 A) and promoted the penetrant formation of de novo centrioles: by 2 d after IAA washout, de novo centriole assembly occurred in 74% of cells and increased to >95% of cells by 4 d after IAA removal (Fig. 6 B and Fig. S4 H). Knockdown of the cartwheel component STIL prevented de novo centriole assembly, suggesting that, similar to canonical centriole duplication, de novo centrioles assemble through a cartwheel-dependent mechanism (Fig. 6 C). Collectively, these data show that Plk4 levels are rate limiting for both canonical and de novo centriole assembly.

De novo centriole assembly occurred stochastically throughout the cytosol of cells, resulting in the formation of a variable number of centrioles (Fig. 6 B and Fig. S4 H). Whereas cells with one to four de novo centrioles always divided normally, cells with supernumerary de novo centrioles underwent frequent (6–18%) multipolar divisions (Fig. 6, D–F). Because the progeny of multipolar divisions are invariably inviable (Ganem et al., 2009), aberrant mitotic divisions are likely to limit the proliferative potential of cells with supernumerary de novo centrioles. The decreased growth potential of cells with supernumerary centrioles may explain why the relative fraction of cells with a normal centriole number gradually increases in abundance after IAA washout (Fig. 6 B).

De novo centriole assembly required cell cycle progression, as arresting cells in G1 phase with mimosine or the CDK2/4 inhibitor PD0332991 greatly reduced the frequency of de novo centriole formation by 2 d after IAA washout (Fig. S5, A–C; Watson et al., 1991; Fry et al., 2004). To examine the composition of de novo centrioles we performed immunostaining for several centriole components at 1, 2, 3, and 4 d after

Published July 6, 2015

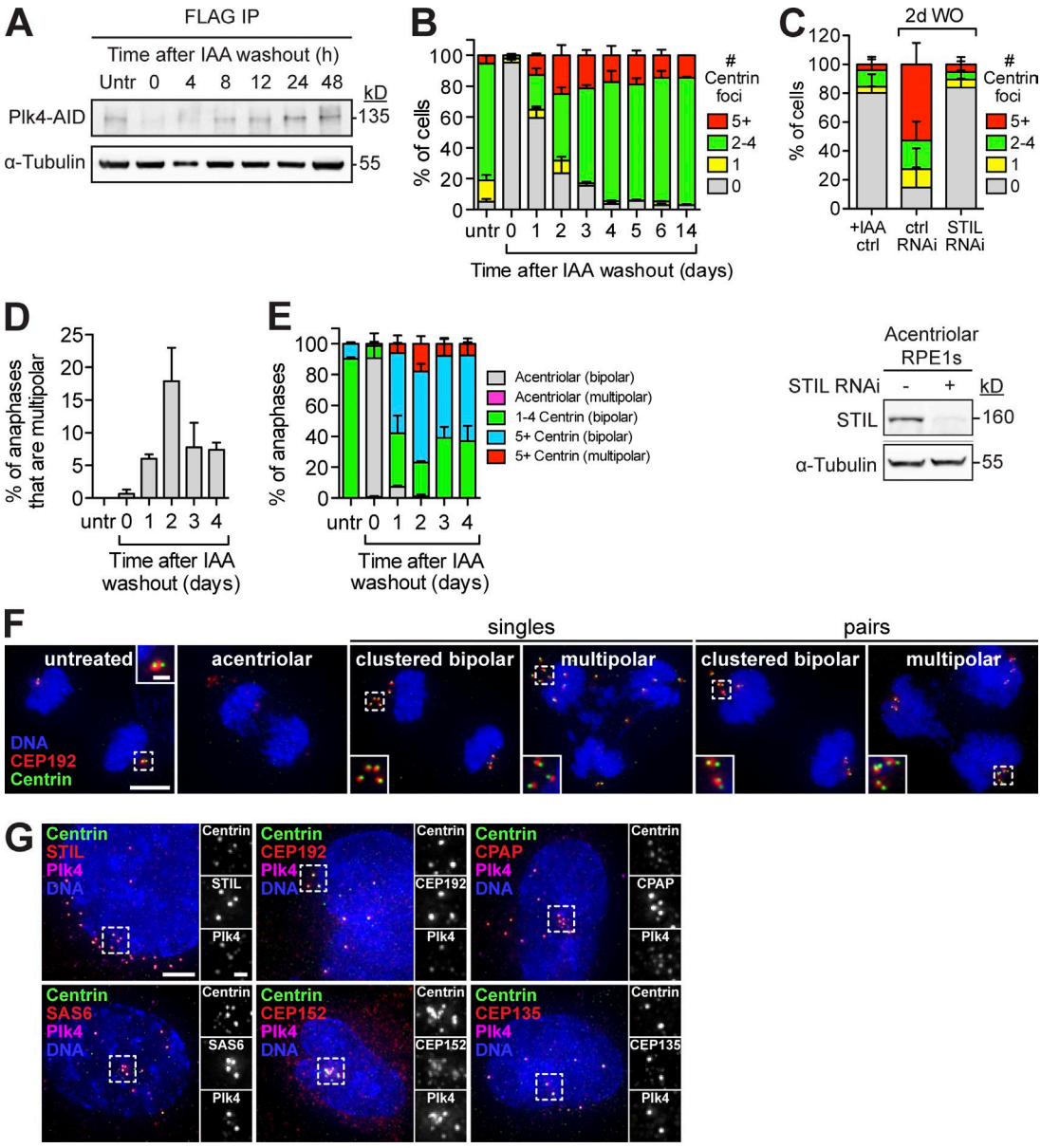


Figure 6. **Restoration of Plk4 levels in acentriolar cells leads to de novo centriole formation.** (A) Immunoblot showing the level of immunoprecipitated endogenous Plk4-AID-FLAG at the indicated times after IAA washout in acentriolar, Plk4$^{AID/AID}$;p53 shRNA cells. (B) Quantification of the number of Centrin foci per interphase cell at indicated times after IAA washout, in Plk4$^{AID/AID}$;p53 shRNA cells. Bars represent the mean of >200 cells from three independent experiments. (C, top) Quantification of the number of Centrin-marked de novo centrioles in interphase cells at 2 d after IAA washout (WO). Cells were transfected with the STIL siRNA 24 h before IAA washout. (bottom) Immunoblot showing depletion of STIL at 48 h after transfection with STIL siRNA. (D and E) Quantification of the fraction of bipolar and multipolar divisions in Plk4$^{AID/AID}$;p53 shRNA at indicated times after IAA washout. Bars represent the mean of >120 cells from two independent experiments. All error bars in the figure represent the SEM. (F) Selected images of anaphase phenotypes. Both single and pairs of de novo centrioles clustered at the poles of the mitotic spindle. Cells were costained with Centrin and CEP192. (G) Selected images of Centrin-marked de novo centrioles at 1 d after IAA washout. Cells were costained with Plk4, STIL, SAS6, CPAP, CEP192, CEP152, and CEP135. Bars: (main) 5 µm; (inset) 1 µm.

IAA washout. By 2 d after IAA washout, Plk4, CPAP, CEP135, CEP152, CEP164, and CEP192 colocalized with at least one Centrin-marked, de novo centriole in >75% of cells (Fig. 6 G and Fig. S5 D). In contrast, only 40–55% of cells with de novo centrioles contained centriole-localized STIL or SAS6, consistent with the fact that STIL and SAS6 are absent from centrioles during G1 phase (Strnad et al., 2007; Tang et al., 2011; Arquint et al., 2012; Arquint and Nigg, 2014). Importantly, all of the de novo centrioles observed in transverse sections by EM exhibited a normal morphology, with triplet microtubules arranged with ninefold rotational symmetry ($n$ = 83 total de novo centrioles, 13 of which were sectioned transversely and could be assessed for rotational symmetry; Fig. 7, A–B).

To examine the kinetics of de novo centriole assembly, we generated acentriolar cells stably expressing EGFP-Centrin and performed time-lapse imaging after IAA washout. Approximately 9 h before mitosis, a variable number of EGFP-Centrin foci formed dispersed throughout the cytosol (Fig. 8, A and B). These foci increased in size and intensity until they were indistinguishable from EGFP-Centrin foci

Published July 6, 2015

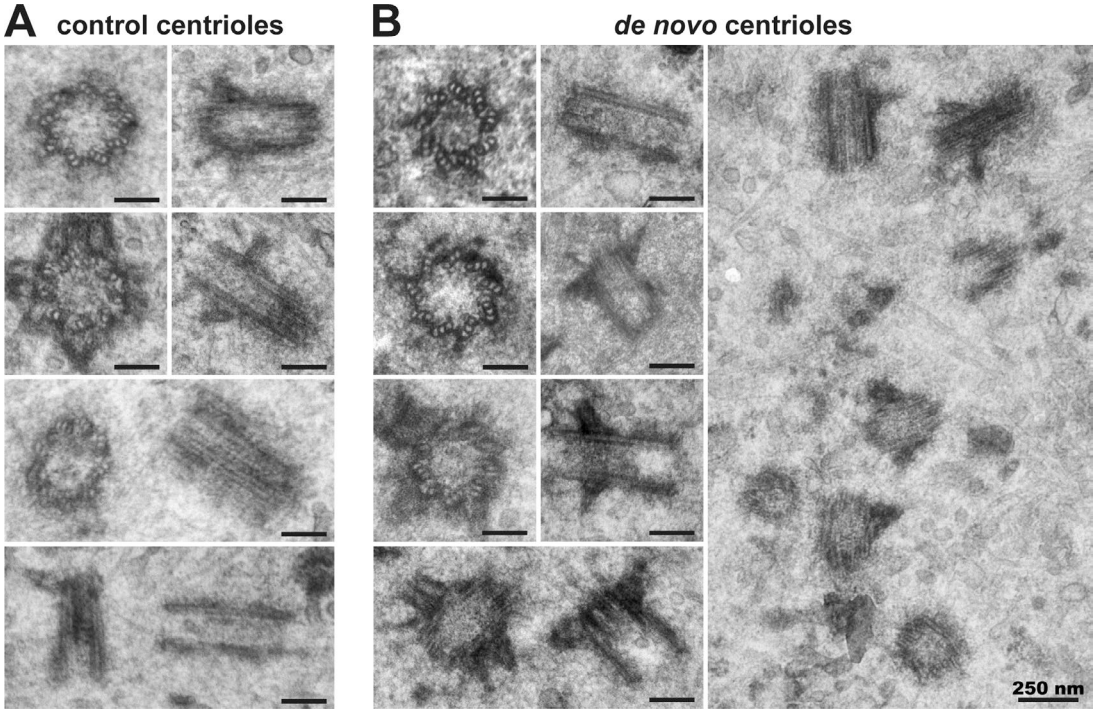


Figure 7. **De novo formed centrioles have a normal structure.** Thin section transmission electron micrographs of existing centrioles (A) or de novo centrioles (B) formed 3 d after IAA washout. Bars, 100 nm, unless indicated otherwise.

observed at normal centrioles in control cells. Immunofluorescence staining showed that the newly formed Centrin foci colocalized with CEP192 and are thus likely to represent de novo centrioles (Fig. 8 C). Once de novo centrioles had formed, no additional Centrin foci were generated, consistent with the observation that de novo centriole assembly is inhibited by the presence of centrioles (Fig. 8 A and Video 5; Marshall et al., 2001; La Terra et al., 2005). To test if a single centriole is capable of suppressing de novo centriole formation, we transiently treated EGFP-Centrin–expressing $Plk4^{AID/AID}$;p53 shRNA cells with IAA to generate a fraction of cells with a single centriole, and then removed IAA and monitored de novo centriole formation by time-lapse microscopy. Strikingly, whereas 80% of acentriolar cells underwent de novo centriole formation within 36 h of IAA washout, only 15% of cells with a single centriole underwent de novo centriole assembly in the same period (Fig. S5 E).

In the first mitotic division after IAA washout, the majority of single de novo centrioles segregated on the mitotic spindle (Fig. 8 D). After the first division, de novo centrioles clustered to a single location. Later in the cell cycle, centrioles dispersed around the nuclear envelope and underwent duplication, with each single EGFP-Centrin focus becoming a duplex of two centrioles (Fig. 8, A and C; and Video 6). Pairs of Centrin foci contained a single focus of the proximal centriole marker CNAP1, consistent with an engaged "mother–daughter" configuration (Fig. 8 E). CEP164 is a distal appendage protein that usually marks the mature mother centriole (Graser et al., 2007). Surprisingly, however, duplicated pairs of de novo centrioles did not always contain a CEP164-positive centriole (Fig. S5 F). By 2 d after IAA washout, duplicated centriole pairs recruited PCM and acted as MTOCs (Fig. 8 D). We conclude that the de novo centrioles are functionally indistinguishable from canonical centrioles.

## Discussion

In this study, we have developed a chemical genetic approach to reversibly deplete Plk4 and centrioles in a proliferating population of human cells. This is the first time the auxin-inducible destruction system has been used to reversibly manipulate the levels of an endogenous protein in vertebrate cells. In principle, the strategy we have taken could be applied to control the levels of many proteins that are not amenable to traditional chemical inhibition. In the future, combining the AID system with CRISPR/Cas9 genome engineering will greatly increase the efficiency with which biallelic targeting of endogenous genes can be achieved, paving the way for rapid and tunable control of protein function.

The long-term consequence of centriole depletion has not been studied in a nontransformed vertebrate cell line. By inducing chronic depletion of Plk4, we reveal the presence of a p53-dependent pathway that arrests the growth of untransformed cells after a failure of centriole duplication (Fig. 5 A). Furthermore, by exploiting the reversibility of Plk4 depletion, we show that the cell cycle arrest caused by centriole loss is irreversible (Fig. 3 C). A recent study arrived at similar conclusions using a potent inhibitor of Plk4 kinase activity to deplete centrioles from proliferating cells (Wong et al., 2015). Mouse embryos lacking the essential centriole protein CPAP lack centrioles and cilia and die during midgestation because of widespread p53-dependent apoptosis (Bazzi and Anderson, 2014). Similarly, deletion of CPAP in the developing mouse brain also resulted in increased cell death, which was rescued by removal of p53 (Insolera et al., 2014). The contrast between the apoptotic response in mouse embryos and the arrest we observed in human cells suggests that embryonic and adult cell types have different proclivities for initiating apoptosis or senescence after centriole loss. Interestingly, in contrast to the situation in mouse and human cells, *Drosophila melano-*

Published July 6, 2015

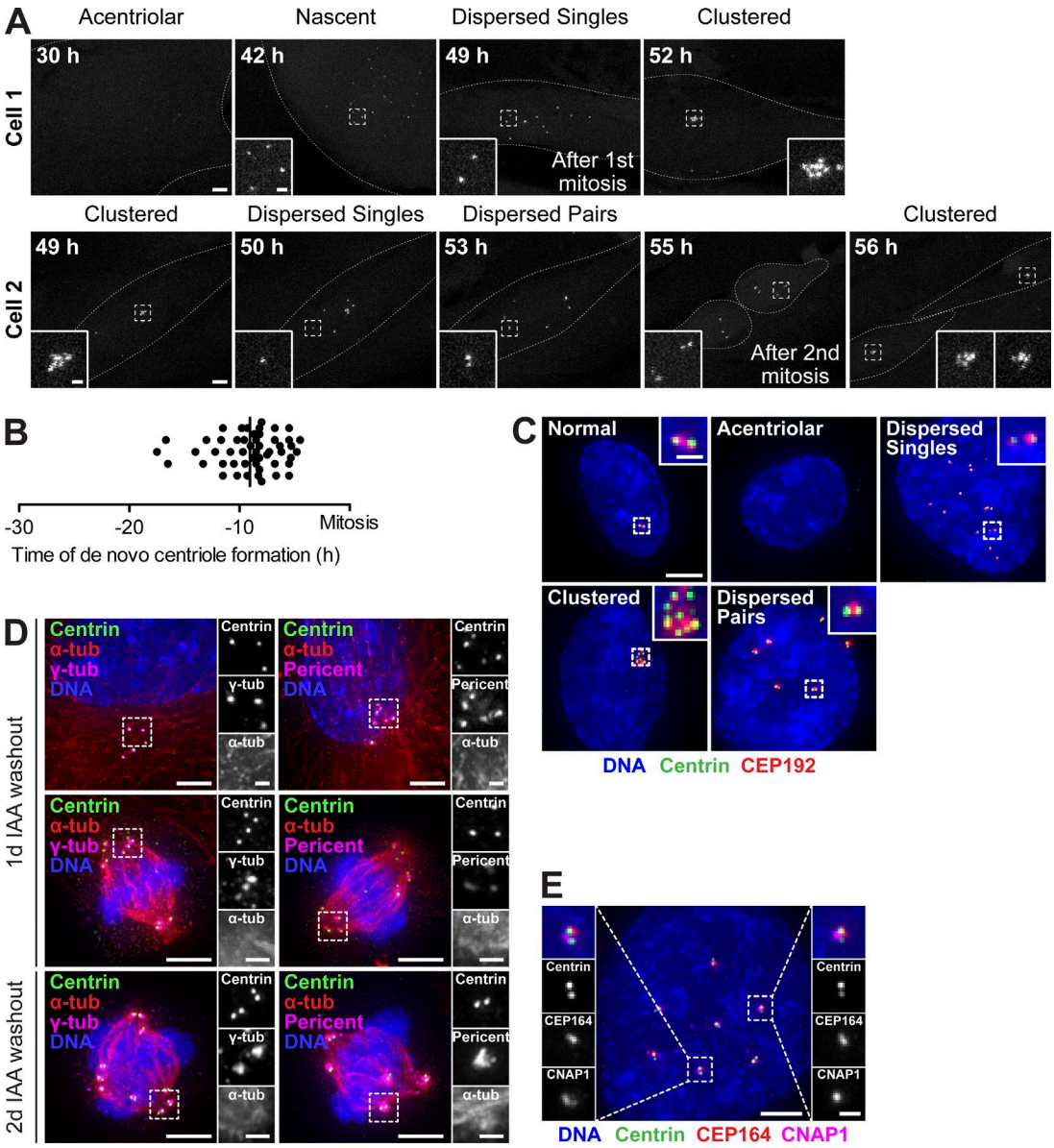


Figure 8. **De novo centrioles recruit PCM and act as MTOCs.** (A) Selected images from a time-lapse series showing de novo centriole formation in cells expressing histone EGFP-Centrin. De novo centrioles duplicate in the second cycle after they are born. Time is indicated in hours relative to the time of IAA washout (time point 0). (B) Quantification of the time of de novo centriole formation relative to the time of cell division. Measurements were made using time-lapse movies of EGFP-Centrin expressing cells from two independent experiments. Line represents the mean of >50 cells. (C) Selected images illustrating the different configurations adopted by de novo centrioles. Cells were costained with Centrin and CEP192 to identify centrioles. (D) Selected images of de novo centrioles in interphase and mitotic cells at 1 and 2 d after IAA washout. The mitotic spindle segregates freestanding de novo centrioles in the first division and pairs of replicated centrioles in the second cell division. Cells were costained with α-tubulin, Centrin, and γ-tubulin or Pericentrin. (E) Selected images of pairs of de novo centrioles in interphase cells at 2 d after IAA washout. Cells were costained with Centrin, CNAP1, and CEP164. Bars: (main) 5 µm; (inset) 1 µm.

*gaster* cells lacking centrioles do not arrest or die (Basto et al., 2006; Lecland et al., 2013), suggesting that cell cycle checkpoints for eliminating acentriolar cells are more stringent in vertebrates.

Whereas mouse embryos proceed through many cell divisions without centrioles before initiating apoptosis, we found that many human somatic cells ceased dividing before the total loss of centrioles (Fig. 4 B). Importantly, we did not observe detectable increases in Hippo pathway activation, DNA damage, or cytokinesis failure in the two to three cell cycles that occur after Plk4 degradation (Figs. 3 E and 4 E). We did, however, observe an increase in chromosome segregation errors in cells with a reduced centriole number (9% at day 1, 19% at day 2, and 14% at day 3 after IAA addition; Fig. 3 E). Although chromosome segregation errors can lead to a p53-dependent arrest (Thompson and Compton, 2010), the frequency of these errors was too low to account for the reduction in proliferation after Plk4 loss (Fig. 3 E). In mouse embryos that lack centrioles, the stabilization of p53 was proposed to arise as a result of a modest (~10 min) increase in mitotic duration (Bazzi and Anderson, 2014). However, using single-cell lineage tracing, we show that an extended mitosis cannot, by itself, explain the cell cycle arrest that occurs in human cells that fail centriole duplication (Fig. 4 D). Further investigation will therefore be required to establish the underlying cause of the proliferative arrest that occurs after Plk4 loss.

Published July 6, 2015

Removal of p53 allowed human cells to proliferate indefinitely despite the absence of centrioles (Fig. 5 A). As centrosomes increase the speed of spindle assembly, these acentriolar cells formed bipolar spindles at a considerably slower rate than cells containing centrioles. In addition, acentriolar cells displayed chromosomal instability and frequent cytokinesis failure (Fig. 5 D). Similar mitotic errors have been reported in acentriolar *D. melanogaser* cells and transformed vertebrate cell lines, highlighting the important role of centrioles in ensuring the fidelity of cell division in adult cells (Khodjakov and Rieder, 2001; Basto et al., 2006; Debec et al., 2010; Sir et al., 2013). Surprisingly, however, acentriolar mouse embryos showed no detectable increase in chromosome segregation errors (Bazzi and Anderson, 2014). The first five rounds of cell division in the mouse embryo are naturally acentriolar (Szollosi et al., 1972) and it is therefore possible that mouse embryonic divisions are less dependent on centrioles for faithful chromosome segregation.

Overexpression of Plk4 did not promote de novo centriole formation in acentriolar mouse zygotes (Coelho et al., 2013), but was capable of inducing de novo centriole formation in unfertilized fly eggs (Peel et al., 2007; Rodrigues-Martins et al., 2007) and activated *Xenopus laevis* oocytes (Eckerdt et al., 2011). Here we have shown that restoring endogenous levels of Plk4 induces de novo centriole formation in acentriolar human somatic cells. We speculate that de novo centrioles are created from Plk4 foci that form stochastically in the cytosol of acentriolar cells (Fig. S5 G). Once these foci surpass a threshold level of Plk4 activity, cartwheel assembly would be initiated, leading to centriole formation. Consistent with this idea, we were able to observe recruitment of the cartwheel components STIL and SAS6 to Plk4 foci as an early event occurring before incorporation of Centrin into de novo centrioles (Fig. S5 G).

De novo centrioles assembled very efficiently (within two to three cell cycles) after restoration of Plk4 levels (Fig. 6 B). This is in accordance with previous work examining the kinetics of de novo centriole formation in somatic human cells (La Terra et al., 2005; Uetake et al., 2007) and green algae (Marshall et al., 2001). Procentrioles formed in S phase are normally modified during mitosis to activate their ability to recruit PCM and function as MTOCs in the next cell cycle (Wang et al., 2011). In our experiments, cells that lack centrioles undergo a prolonged prometaphase, providing increased time for newly created de novo centrioles to be modified and converted into MTOCs. Consistently, we observed that in the first cell cycle the vast majority of de novo centrioles recruited small amounts of PCM in mitosis and were capable of segregating themselves on the mitotic spindle (Fig. 8 D). De novo centrioles duplicated in the second cell cycle after their creation, consistent with a previous study demonstrating that newly formed centrioles are modified in mitosis to license their duplication (Fig. 8, A and D; Wang et al., 2011).

A single centriole was shown to suppress de novo centriole assembly in the vast majority of cells, supporting the conclusion that existing centrioles inhibit the de novo assembly pathway (Fig. S5 E; Marshall et al., 2001; La Terra et al., 2005). Like canonical centriole assembly, de novo centriole formation requires Plk4 activity (Wong et al., 2015). An intriguing possibility, therefore, is that existing centrioles sequester an activator of Plk4 and thereby act to inhibit the cytosolic pool of Plk4 and suppress de novo centriole formation. The ability to induce timed de novo centriole biogenesis in populations of cycling acentriolar cells offers an excellent tool to dissect the molecular events involved in centriole formation and how existing centrioles antagonize the de novo pathway.

## Materials and methods

### Antibody production

A C-terminal Plk4 fragment (aa 510–970) was cloned into a pET-23b bacterial expression vector (EMD Millipore) containing a C-terminal 6xHis tag. Recombinant protein was purified from *Escherichia coli* using Ni-NTA beads (QIAGEN) and used for immunization (ProSci). A STIL C-terminal peptide VGTFLDVKRLRQLPKLF (aa 1,271–1,287) was synthesized and conjugated to KLH for immunization. Rabbit immune sera were affinity purified using standard procedures. Affinity purified antibodies were directly conjugated to DyLight 550 and DyLight 650 fluorophores (Thermo Fisher Scientific) for use in immunofluorescence.

### Cell culture

hTERT RPE-1 cells were maintained at 37°C in a 5% $CO_2$ atmosphere with 21% oxygen. Cells were grown in DMEM/F12 medium containing 10% fetal bovine serum (Sigma-Aldrich), 0.348% sodium bicarbonate, 100 U/ml penicillin, 100 U/ml streptomycin, and 2 mM L-glutamine. Nocodazole (Sigma-Aldrich) was dissolved in DMSO and used at a final concentration of 3.3 µM; Mimosine (Sigma-Aldrich) was dissolved in diluted HCl and used at a final concentration of 250 µM; PD0332991 (Sigma-Aldrich) was dissolved in DMSO and used at a final concentration of 1 µM; SB203580 (Sigma-Aldrich) was dissolved in DMSO and used at a final concentration of 10 µM; Doxorubicin (Sigma-Aldrich) was dissolved in water and used at a final concentration of 200 ng/ml; and IAA (Sigma-Aldrich) was dissolved in water and used at 500 µM unless otherwise stated.

### Gene targeting and stable cell lines

Gene targeting was performed using adeno-associated virus (AAV; Berdougo et al., 2009; Holland et al., 2012b). To generate the Plk4 targeting construct we cloned an AID degron followed by a 3xFLAG epitope tag, a translational stop codon, the Plk4 3′ UTR, and 150 bp of adjacent genomic sequence into the pBluescript derivative pNY to create the AID-3xFLAG-3′UTR;*loxP*-Neo$^R$-*loxP* vector. 5′ and 3′ homology arms were PCR amplified from genomic RPE1 DNA and cloned on either side of the central AID-3xFLAG-3′UTR;*loxP*-Neo$^R$-*loxP* cassette. The entire insert was transferred into the pAAV vector backbone and fully sequenced to verify its integrity. hTERT-RPE1 cells were transduced with infectious AID-3xFLAG-3′UTR;*loxP*-Neo$^R$-*loxP*–containing AAV particles. Plk4$^{AID/+}$ cells were isolated by selection in G418 and resistant clones were screened by PCR using primers binding in Neo$^R$ and a genomic sequence adjacent to the targeting construct. A second targeting construct was created containing a HA tag in place of the FLAG epitope tag and a Blast$^R$ in place of Neo$^R$. An additional round of gene targeting was performed in Plk4$^{AID/+}$ cells using AID-HA-3′UTR;*loxP*-Blast$^R$-*loxP* AAV particles. The intergenic position of the Neo$^R$ and Blast$^R$ cassettes reduces the likelihood that their presence will disrupt the function of the Plk4 gene. This facilitates the isolation of homozygous targeted alleles by allowing concurrent selection for both markers. Plk4$^{AID/AID}$ cells were isolated by coselection in G418 and blasticidin and resistant clones were screened by PCR using primers that bind in Blast$^R$ and a genomic sequence adjacent to the targeting construct. Two independent Plk4$^{AID/AID}$ clones were created and the targeted Plk4-AID-3xFLAG and Plk4-AID-3xHA alleles were sequenced to verify their integrity. osTIR1-9xMyc was cloned into the pBabe backbone under the control of the gag promoter and introduced into Plk4$^{AID/AID}$ cells using retroviral delivery.

Published July 6, 2015

Stable integrants were selected in 5 µg/ml puromycin and single clones were isolated by limiting dilution. EGFP-tagged Cep63 was cloned into the FUGW backbone under the control of the ubiquitin promoter, whereas EGFP-tagged histone H2B and TagRFP-tubulin were cloned into the FUGW backbone under the control of the CMV promoter. All three constructs were introduced into $Plk4^{AID/AID}$ cells using lentiviral delivery and single clones were isolated by limiting dilution. A p53 shRNA was introduced into cells using lentiviral delivery and single clones were isolated using fluorescence-activated cell sorting (Tiscornia et al., 2003).

### Antibody techniques

To purify Plk4-AID-3xFLAG, cells were lysed in lysis buffer (10 mM Tris, pH 7.5, 0.1% Triton X-100, 100 mM NaCl, 1 mM EDTA, 1 mM EGTA, 50 mM NaF, 20 mM, β-glycerophosphate, 0.1 mM DTT, 200 nM microcystin, 1 mM PMSF, and 1 µM LPC) and sonicated and soluble extracts were prepared. The supernatant was incubated with anti-FLAG M2 magnetic beads (Sigma-Aldrich). Beads were washed five times in lysis buffer and immunopurified protein was analyzed by immunoblot.

For immunoblot analysis, protein samples were separated by SDS-PAGE, transferred onto nitrocellulose membranes with a Trans-Blot Turbo Transfer System (Bio-Rad Laboratories), and then probed with the following antibodies: DM1A (mouse anti–α-tubulin, 1:5,000; Sigma-Aldrich), Plk4 (rabbit, 1:3,200; this study), FLAG M2 (mouse, 1:1,000; Sigma-Aldrich), STIL (rabbit, 1:2,500; Bethyl Laboratories, Inc.), Yap (rabbit, 1:1,000, Cell Signaling Technology), p-Yap Ser127 (rabbit, 1:1,000; Cell Signaling Technology), LATS2 (rabbit, 1:1,000; Cell Signaling Technology), p-LATS S1077 (rabbit, 1:500; Yu et al., 2010; a gift of D. Pan, Johns Hopkins School of Medicine, Baltimore, MD), and p-Histone H2A.X (Ser139; rabbit, 1:1,000; Cell Signaling Technology).

For immunofluorescence, cells were grown on 18-mm glass coverslips and fixed in 100% ice-cold methanol for 10 min. Cells were blocked in 2.5% FBS, 200 mM glycine, and 0.1% Triton X-100 in PBS for 1 h. Antibody incubations were conducted in the blocking solution for 1 h. DNA was detected using DAPI and cells were mounted in Prolong Antifade (Invitrogen). Staining was performed with the following primary antibodies: GTU-88 (mouse anti–γ-tubulin, 1:250; Abcam), Centrin (mouse, 1:1,000; EMD Millipore), CNAP1 (guinea pig, raised against the CNAP1 peptide sequence SPTQQDGRGQKNSDAKC, 1:1,000, a gift from O. Stemmann, University of Bayreuth, Bayreuth, Germany), CEP152 (rabbit, 1:5,000; Bethyl Laboratories, Inc.), Plk4-650 (directly labeled rabbit, 1:1,000; this study), STIL-550 (directly labeled rabbit, 1:1,000; this study), CEP135 (rabbit, raised against CEP135 aa 695–838, 1:1,000; a gift from A. Hyman, Max Planck Institute for Molecular Cell Biology and Genetics, Dresden, Germany), CEP192-Cy3 (directly labeled rabbit, raised against CEP192 aa 1–211, 1:1,000; a gift from K. Oegema, Ludwig Institute for Cancer Research, La Jolla, CA), SAS6-Cy3 (directly labeled rabbit, raised against SAS6 aa 501–657, 1:1,000, a gift from K. Oegema), SAS6 (mouse, 1:1,000; Santa Cruz Biotechnology, Inc.), CPAP-Cy3 (directly labeled rabbit, 1:1,000; a gift from K. Oegema), CENP-F (sheep, raised against CENP-F aa 1,363–1,640, 1:1,000; a gift from S. Taylor, University of Manchester, Manchester, UK), HA (rat anti-HA High Affinity, 1:200; Roche), and FLAG (mouse anti-FLAG M2, 1:1,000; Sigma-Aldrich). Secondary donkey antibodies were conjugated to Alexa Fluor 488, 555, or 650 (Life Technologies). To mark S phase, cells were pulsed with EdU before fixation in 100% ice-cold methanol at −20°C for 10 min. Cells were washed three times with 0.1% Triton X-100 in PBS and stained using a Click-It EdU Alexa Fluor 555 imaging kit (Life Technologies) according to the manufacturer's recommendations.

For the cell cycle analysis of Plk4 levels shown in Fig. 1 E, cells were pulsed with EdU for 1 h before fixation in 100% ice-cold methanol at −20°C for 10 min. Cells were washed three times with 0.1% Triton X-100, stained using a Click-It EdU Alexa Fluor 555 imaging kit (Life Technologies), and blocked in 2.5% FBS, 200 mM glycine, and 0.1% Triton X-100 in PBS for 1 h. Immunofluorescence microscopy was performed using the following antibodies: CENP-F (sheep, raised against CENP-F aa 1,363–1,640, 1:1,000; a gift from S. Taylor), GTU-88 (mouse anti–γ-tubulin, 1:250; Abcam), and Plk4-650 (directly labeled rabbit, 1:1,000; this study). G1 phase cells were classified as CENP-F and EdU negative, S phase cells were classified as EdU positive, and G2 phase cells were classified as CENP-F positive and EdU negative. The γ-tubulin staining was used to define the position of the centrosome.

Immunofluorescence images were collected using a Deltavision Elite system (GE Healthcare) controlling a camera (pco.edge 5.5; Scientific CMOS). Acquisition parameters were controlled by SoftWoRx suite (GE Healthcare). Images were collected at room temperature (25°C) using a 40× 1.35 NA, 60× 1.42 NA, or 100× 1.4 NA oil objective (Olympus) at 0.2-µm z-sections and subsequently deconvolved in SoftWoRx suite. Images were acquired using immersion oil ($n$ = 1.516; Applied Precision). For quantitation of signal intensity at the centrosome, deconvolved 2D maximum intensity projections were saved as 16-bit TIFF images. Signal intensity was determined using ImageJ by drawing a circular region of interest (ROI) around the centriole (ROI S). A larger concentric circle (ROI L) was drawn around ROI S. ROI S and L were transferred to the channel of interest and the signal in ROI S was calculated using the formula IS − [(IL − IS/AL − AS) × AS], where A is area and I is integrated pixel intensity.

### Live-cell microscopy

Cells were seeded into four-chamber, 35-mm glass bottom culture dishes (Greiner) and maintained at 37°C in an environmental control station. Images were collected using a Deltavision Elite system controlling a camera (pco.edge 5.5.). Images were acquired with a 40× 1.35 NA oil lens using immersion oil ($n$ = 1.526). Every 5 min, 7 × 3-µm z-sections were acquired for EGFP and RFP and maximum intensity projection was created using SoftWoRx. Alternatively, cells were imaged using a 40× 1.4 NA Plan Apochromat oil-immersion objective (Carl Zeiss) on a confocal microscope (LSM 780; Carl Zeiss) equipped with a solid-state 488- and 514-nm laser and a spectral GaAsP detector. Images were acquired using immersion oil ($n$ = 1.518; Carl Zeiss). Acquisition parameters, shutters, and focus were controlled by ZEN black software (Carl Zeiss). 15 × 1.6-µm z-sections were acquired simultaneously for EGFP and/or RFP at 5- or 10-min time intervals. Maximum intensity projections were created using ZEN black. Movies were assembled and analyzed using FIJI.

### Lineage tracing

For nocodazole treatment, coverslips were assembled into observation chambers with medium containing 0.08 µM nocodazole and fields of cells were continuously followed by video time-lapse microscopy at 37°C for 6 h. After 6 h, the field of view was marked with a diamond scribe; the bottom of the observation chamber was removed and washed out with fresh medium several times before being reassembled with fresh medium as previously described (Uetake and Sluder, 2012). The previously marked fields were continuously followed for at least 96 h. Lineage tracing of individual cells was performed as previously described (Uetake et al., 2007). For IAA and SB203580 treatment, cells were exposed to the drug for the duration of imaging. Images were collected using a microscope (DMRXE; Leica) equipped with phase-contrast optics and a 10× 0.3 NA objective (Leica). Images were captured with an Orca ER (Hamamatsu Photonics) camera using HCT software (Hamamatsu Photonics) and exported as AVI movies to be viewed with QuickTime (Apple).

Published July 6, 2015

### EM

Cells were grown on 35-mm Nunclon Delta–treated culture dishes (Thermo Fisher Scientific) and fixed (2.5% glutaraldehyde, 3 mM $MgCl_2$, and 0.1 M sodium cacodylate, pH 7.2) for 1 h at room temperature. Cells were rinsed with 0.1 M sodium cacodylate and post-fixed with 0.5% $OsO_4$ for 1 h on ice. After a $dH_2O$ rinse, plates were stained with 0.1% tannic acid, rinsed twice with $dH_2O$, and stained en bloc with 2% aqueous uranyl acetate. Samples were dehydrated in a graded series of ethanol, embedded in Eponate 12 resin (Ted Pella), and polymerized at 60°C overnight. Ultrathin 60-nm sections were cut, mounted, and stained with 1% tannic acid, followed by 2% uranyl acetate and lead citrate. Images were acquired using a transmission electron microscope (7600; Hitachi) equipped with a charge coupled device 2,080 × 2,048-pixel camera (Advanced Microscopy Techniques).

### Cell biology

To prepare cells for flow cytometry, cell pellets were fixed in cold 70% EtOH for 24 h, washed once in PBS, and resuspended in PBS supplemented with 0.5 mg/ml RNase A and 50 mg/ml propidium iodide. Samples were incubated at room temperature for 30 min and analyzed on a flow cytometer (FACSCalibur; BD). For RNA interference, $2 \times 10^5$ cells were seeded in a 6-well plate and duplexed siRNAs were introduced using RNAiMax (Life Technologies). siRNA directed against STIL (5′-GCUCCAAACAGUUUCUGCUGGAAU-3′) was purchased from GE Healthcare.

### Online supplemental material

Fig. S1 shows the strategy for the generation of $Plk4^{AID/AID}$ cells and that Plk4 destruction occurs rapidly in an osTIR1-dependent manner. Fig. S2 shows that Plk4 destruction dramatically reduces clonogenic survival and that treatment of parental RPE1 cells with IAA does not alter mitotic timing. Fig. S3 shows that $Plk4^{AID/AID}$ cells have a window of prometaphase tolerance of 97 min, that IAA treatment reduces the window of hTERT RPE1 cells to 60 min, and that inhibition of p38 MAPK activity with SB203580 does not prevent the cell cycle arrest that occurs as a result of centriole duplication failure. Fig. S4 shows that p53 is stabilized after Plk4 destruction, that depletion of p53 partially rescues the clonogenic survival of cells lacking Plk4, that mitotic spindles form in the absence of centrioles, and that the incidence of polyploidy increases in acentriolar cells. Fig. S5 shows that de novo centrioles do not form in G1-arrested cells, that the composition of de novo centrioles is similar at 1–4 d after their assembly, and that a single existing centriole is capable of suppressing de novo centriole formation. Video 1 shows a normal cell division in an untreated $Plk4^{AID/AID}$ cell. Video 2 shows an IAA-treated $Plk4^{AID/AID}$ cell dividing with an asymmetric spindle. Video 3 shows a normal cell division in an untreated $Plk4^{AID/AID}$;p53 shRNA cell. Video 4 shows a $Plk4^{AID/AID}$;p53 shRNA cell dividing without centrioles. Video 5 shows de novo centriole formation after recovery of Plk4 levels. Video 6 shows duplication of de novo formed centrioles. Online supplemental material is available at http://www.jcb.org/cgi/content/full/jcb.201502089/DC1.

## Acknowledgments

The authors would like to thank Stephen Taylor for providing the sheep CENP-F antibody, Anthony Hyman for providing the CEP135 antibody, Duojia Pan for providing the p-LATS S1077 antibody, Olaf Stemmann for providing the CNAP1 antibody, and Karen Oegema for providing the CEP192, CPAP, and SAS6 antibodies. We thank Barbara Smith and the Johns Hopkins School of Medicine Microscope Facility for help with EM analysis. We thank the Johns Hopkins Center for Sensory Biology/Hearing and Balance imaging center for use of their confocal microscope. We thank Michelle Levine and Randall Reed for comments on the manuscript.

This work was supported by the Leukemia Research Foundation, a W.W. Smith Charitable Trust Research Grant, a March of Dimes Basil O'Conner Scholar Award, a Pew Scholar Award, a Kimmel Scholar Award, and research grants GM 114119 (to A.J. Holland) and GM 30758 (to G. Sluder) from the National Institutes of Health.

The authors declare no competing financial interests.

Submitted: 24 February 2015
Accepted: 1 June 2015

## References

Arquint, C., and E.A. Nigg. 2014. STIL microcephaly mutations interfere with APC/C-mediated degradation and cause centriole amplification. *Curr. Biol.* 24:351–360. http://dx.doi.org/10.1016/j.cub.2013.12.016

Arquint, C., K.F. Sonnen, Y.D. Stierhof, and E.A. Nigg. 2012. Cell-cycle-regulated expression of STIL controls centriole number in human cells. *J. Cell Sci.* 125:1342–1352. http://dx.doi.org/10.1242/jcs.099887

Basto, R., J. Lau, T. Vinogradova, A. Gardiol, C.G. Woods, A. Khodjakov, and J.W. Raff. 2006. Flies without centrioles. *Cell.* 125:1375–1386. http://dx.doi.org/10.1016/j.cell.2006.05.025

Bazzi, H., and K.V. Anderson. 2014. Acentriolar mitosis activates a p53-dependent apoptosis pathway in the mouse embryo. *Proc. Natl. Acad. Sci. USA.* 111:E1491–E1500. http://dx.doi.org/10.1073/pnas.1400568111

Berdougo, E., M.E. Terret, and P.V. Jallepalli. 2009. Functional dissection of mitotic regulators through gene targeting in human somatic cells. *Methods Mol. Biol.* 545:21–37.

Bettencourt-Dias, M., A. Rodrigues-Martins, L. Carpenter, M. Riparbelli, L. Lehmann, M.K. Gatt, N. Carmo, F. Balloux, G. Callaini, and D.M. Glover. 2005. SAK/PLK4 is required for centriole duplication and flagella development. *Curr. Biol.* 15:2199–2207. http://dx.doi.org/10.1016/j.cub.2005.11.042

Brownlee, C.W., J.E. Klebba, D.W. Buster, and G.C. Rogers. 2011. The Protein Phosphatase 2A regulatory subunit Twins stabilizes Plk4 to induce centriole amplification. *J. Cell Biol.* 195:231–243. http://dx.doi.org/10.1083/jcb.201107086

Coelho, P.A., L. Bury, B. Sharif, M.G. Riparbelli, J. Fu, G. Callaini, D.M. Glover, and M. Zernicka-Goetz. 2013. Spindle formation in the mouse embryo requires Plk4 in the absence of centrioles. *Dev. Cell.* 27:586–597. http://dx.doi.org/10.1016/j.devcel.2013.09.029

Cunha-Ferreira, I., A. Rodrigues-Martins, I. Bento, M. Riparbelli, W. Zhang, E. Laue, G. Callaini, D.M. Glover, and M. Bettencourt-Dias. 2009. The SCF/Slimb ubiquitin ligase limits centrosome amplification through degradation of SAK/PLK4. *Curr. Biol.* 19:43–49. http://dx.doi.org/10.1016/j.cub.2008.11.037

Cunha-Ferreira, I., I. Bento, A. Pimenta-Marques, S.C. Jana, M. Lince-Faria, P. Duarte, J. Borrego-Pinto, S. Gilberto, T. Amado, D. Brito, et al. 2013. Regulation of autophosphorylation controls PLK4 self-destruction and centriole number. *Curr. Biol.* 23:2245–2254. http://dx.doi.org/10.1016/j.cub.2013.09.037

Debec, A., W. Sullivan, and M. Bettencourt-Dias. 2010. Centrioles: active players or passengers during mitosis? *Cell. Mol. Life Sci.* 67:2173–2194. http://dx.doi.org/10.1007/s00018-010-0323-9

Dzhindzhev, N.S., G. Tzolovsky, Z. Lipinszki, S. Schneider, R. Lattao, J. Fu, J. Debski, M. Dadlez, and D.M. Glover. 2014. Plk4 phosphorylates Ana2 to trigger Sas6 recruitment and procentriole formation. *Curr. Biol.* 24:2526–2532. http://dx.doi.org/10.1016/j.cub.2014.08.061

Eckerdt, F., T.M. Yamamoto, A.L. Lewellyn, and J.L. Maller. 2011. Identification of a polo-like kinase 4-dependent pathway for de novo centriole formation. *Curr. Biol.* 21:428–432. http://dx.doi.org/10.1016/j.cub.2011.01.072

Fry, D.W., P.J. Harvey, P.R. Keller, W.L. Elliott, M. Meade, E. Trachet, M. Albassam, X. Zheng, W.R. Leopold, N.K. Pryer, and P.L. Toogood. 2004. Specific inhibition of cyclin-dependent kinase 4/6 by PD 0332991 and associated antitumor activity in human tumor xenografts. *Mol. Cancer Ther.* 3:1427–1438.

Ganem, N.J., S.A. Godinho, and D. Pellman. 2009. A mechanism linking extra centrosomes to chromosomal instability. *Nature.* 460:278–282. http://dx.doi.org/10.1038/nature08136

Ganem, N.J., H. Cornils, S.Y. Chiu, K.P. O'Rourke, J. Arnaud, D. Yimlamai, M. Théry, F.D. Camargo, and D. Pellman. 2014. Cytokinesis failure triggers

hippo tumor suppressor pathway activation. *Cell.* 158:833–848. http://dx.doi.org/10.1016/j.cell.2014.06.029

Gönczy, P. 2012. Towards a molecular architecture of centriole assembly. *Nat. Rev. Mol. Cell Biol.* 13:425–435. http://dx.doi.org/10.1038/nrm3373

Graser, S., Y.D. Stierhof, S.B. Lavoie, O.S. Gassner, S. Lamla, M. Le Clech, and E.A. Nigg. 2007. Cep164, a novel centriole appendage protein required for primary cilium formation. *J. Cell Biol.* 179:321–330. http://dx.doi.org/10.1083/jcb.200707181

Guderian, G., J. Westendorf, A. Uldschmid, and E.A. Nigg. 2010. Plk4 *trans*-autophosphorylation regulates centriole number by controlling βTrCP-mediated degradation. *J. Cell Sci.* 123:2163–2169. http://dx.doi.org/10.1242/jcs.068502

Habedanck, R., Y.D. Stierhof, C.J. Wilkinson, and E.A. Nigg. 2005. The Polo kinase Plk4 functions in centriole duplication. *Nat. Cell Biol.* 7:1140–1146. http://dx.doi.org/10.1038/ncb1320

Holland, A.J., and D.W. Cleveland. 2014. Polo-like kinase 4 inhibition: a strategy for cancer therapy? *Cancer Cell.* 26:151–153. http://dx.doi.org/10.1016/j.ccr.2014.07.017

Holland, A.J., W. Lan, S. Niessen, H. Hoover, and D.W. Cleveland. 2010. Polo-like kinase 4 kinase activity limits centrosome overduplication by autoregulating its own stability. *J. Cell Biol.* 188:191–198. http://dx.doi.org/10.1083/jcb.200911102

Holland, A.J., D. Fachinetti, S. Da Cruz, Q. Zhu, B. Vitre, M. Lince-Faria, D. Chen, N. Parish, I.M. Verma, M. Bettencourt-Dias, and D.W. Cleveland. 2012a. Polo-like kinase 4 controls centriole duplication but does not directly regulate cytokinesis. *Mol. Biol. Cell.* 23:1838–1845. http://dx.doi.org/10.1091/mbc.E11-12-1043

Holland, A.J., D. Fachinetti, Q. Zhu, M. Bauer, I.M. Verma, E.A. Nigg, and D.W. Cleveland. 2012b. The autoregulated instability of Polo-like kinase 4 limits centrosome duplication to once per cell cycle. *Genes Dev.* 26:2684–2689. http://dx.doi.org/10.1101/gad.207027.112

Hussein, D., and S.S. Taylor. 2002. Farnesylation of Cenp-F is required for G2/M progression and degradation after mitosis. *J. Cell Sci.* 115:3403–3414.

Insolera, R., H. Bazzi, W. Shao, K.V. Anderson, and S.H. Shi. 2014. Cortical neurogenesis in the absence of centrioles. *Nat. Neurosci.* 17:1528–1535. http://dx.doi.org/10.1038/nn.3831

Izquierdo, D., W.J. Wang, K. Uryu, and M.F. Tsou. 2014. Stabilization of cartwheel-less centrioles for duplication requires CEP295-mediated centriole-to-centrosome conversion. *Cell Reports.* 8:957–965. http://dx.doi.org/10.1016/j.celrep.2014.07.022

Khodjakov, A., and C.L. Rieder. 2001. Centrosomes enhance the fidelity of cytokinesis in vertebrates and are required for cell cycle progression. *J. Cell Biol.* 153:237–242. http://dx.doi.org/10.1083/jcb.153.1.237

Khodjakov, A., C.L. Rieder, G. Sluder, G. Cassels, O. Sibon, and C.L. Wang. 2002. De novo formation of centrosomes in vertebrate cells arrested during S phase. *J. Cell Biol.* 158:1171–1181. http://dx.doi.org/10.1083/jcb.200205102

Kitagawa, D., I. Vakonakis, N. Olieric, M. Hilbert, D. Keller, V. Olieric, M. Bortfeld, M.C. Erat, I. Flückiger, P. Gönczy, and M.O. Steinmetz. 2011. Structural basis of the 9-fold symmetry of centrioles. *Cell.* 144:364–375. http://dx.doi.org/10.1016/j.cell.2011.01.008

Klebba, J.E., D.W. Buster, A.L. Nguyen, S. Swatkoski, M. Gucek, N.M. Rusan, and G.C. Rogers. 2013. Polo-like kinase 4 autodestructs by generating its Slimb-binding phosphodegron. *Curr. Biol.* 23:2255–2261. http://dx.doi.org/10.1016/j.cub.2013.09.019

Ko, M.A., C.O. Rosario, J.W. Hudson, S. Kulkarni, A. Pollett, J.W. Dennis, and C.J. Swallow. 2005. Plk4 haploinsufficiency causes mitotic infidelity and carcinogenesis. *Nat. Genet.* 37:883–888. http://dx.doi.org/10.1038/ng1605

La Terra, S., C.N. English, P. Hergert, B.F. McEwen, G. Sluder, and A. Khodjakov. 2005. The de novo centriole assembly pathway in HeLa cells: cell cycle progression and centriole assembly/maturation. *J. Cell Biol.* 168:713–722. http://dx.doi.org/10.1083/jcb.200411126

Lecland, N., A. Debec, A. Delmas, S. Moutinho-Pereira, N. Malmanche, A. Bouissou, C. Dupré, A. Jourdan, B. Raynaud-Messina, H. Maiato, and A. Guichet. 2013. Establishment and mitotic characterization of new *Drosophila* acentriolar cell lines from DSas-4 mutant. *Biol. Open.* 2:314–323. http://dx.doi.org/10.1242/bio.20133327

Liu, L., C.Z. Zhang, M. Cai, J. Fu, G.G. Chen, and J. Yun. 2012. Downregulation of polo-like kinase 4 in hepatocellular carcinoma associates with poor prognosis. *PLoS ONE.* 7:e41293. http://dx.doi.org/10.1371/journal.pone.0041293

Marshall, W.F., Y. Vucica, and J.L. Rosenbaum. 2001. Kinetics and regulation of de novo centriole assembly. Implications for the mechanism of centriole duplication. *Curr. Biol.* 11:308–317. http://dx.doi.org/10.1016/S0960-9822(01)00094-X

Mason, J.M., D.C. Lin, X. Wei, Y. Che, Y. Yao, R. Kiarash, D.W. Cescon, G.C. Fletcher, D.E. Awrey, M.R. Bray, et al. 2014. Functional characterization of CFI-400945, a Polo-like kinase 4 inhibitor, as a potential anticancer agent. *Cancer Cell.* 26:163–176. http://dx.doi.org/10.1016/j.ccr.2014.05.006

Miki-Noumura, T. 1977. Studies on the de novo formation of centrioles: aster formation in the activated eggs of sea urchin. *J. Cell Sci.* 24:203–216.

Nigg, E.A., and J.W. Raff. 2009. Centrioles, centrosomes, and cilia in health and disease. *Cell.* 139:663–678. http://dx.doi.org/10.1016/j.cell.2009.10.036

Nishimura, K., T. Fukagawa, H. Takisawa, T. Kakimoto, and M. Kanemaki. 2009. An auxin-based degron system for the rapid depletion of proteins in nonplant cells. *Nat. Methods.* 6:917–922. http://dx.doi.org/10.1038/nmeth.1401

Ohta, M., T. Ashikawa, Y. Nozaki, H. Kozuka-Hata, H. Goto, M. Inagaki, M. Oyama, and D. Kitagawa. 2014. Direct interaction of Plk4 with STIL ensures formation of a single procentriole per parental centriole. *Nat. Commun.* 5:5267. http://dx.doi.org/10.1038/ncomms6267

Palazzo, R.E., E. Vaisberg, R.W. Cole, and C.L. Rieder. 1992. Centriole duplication in lysates of *Spisula solidissima* oocytes. *Science.* 256:219–221. http://dx.doi.org/10.1126/science.1566068

Peel, N., N.R. Stevens, R. Basto, and J.W. Raff. 2007. Overexpressing centriole-replication proteins in vivo induces centriole overduplication and de novo formation. *Curr. Biol.* 17:834–843. http://dx.doi.org/10.1016/j.cub.2007.04.036

Pellegrino, R., D.F. Calvisi, S. Ladu, V. Ehemann, T. Staniscia, M. Evert, F. Dombrowski, P. Schirmacher, and T. Longerich. 2010. Oncogenic and tumor suppressive roles of polo-like kinases in human hepatocellular carcinoma. *Hepatology.* 51:857–868.

Rodrigues-Martins, A., M. Riparbelli, G. Callaini, D.M. Glover, and M. Bettencourt-Dias. 2007. Revisiting the role of the mother centriole in centriole biogenesis. *Science.* 316:1046–1050. http://dx.doi.org/10.1126/science.1142950

Rogers, G.C., N.M. Rusan, D.M. Roberts, M. Peifer, and S.L. Rogers. 2009. The $SCF^{Slimb}$ ubiquitin ligase regulates Plk4/Sak levels to block centriole reduplication. *J. Cell Biol.* 184:225–239. http://dx.doi.org/10.1083/jcb.200808049

Silkworth, W.T., I.K. Nardi, L.M. Scholl, and D. Cimini. 2009. Multipolar spindle pole coalescence is a major source of kinetochore mis-attachment and chromosome mis-segregation in cancer cells. *PLoS ONE.* 4:e6564. http://dx.doi.org/10.1371/journal.pone.0006564

Sir, J.H., A.R. Barr, A.K. Nicholas, O.P. Carvalho, M. Khurshid, A. Sossick, S. Reichelt, C. D'Santos, C.G. Woods, and F. Gergely. 2011. A primary microcephaly protein complex forms a ring around parental centrioles. *Nat. Genet.* 43:1147–1153. http://dx.doi.org/10.1038/ng.971

Sir, J.H., M. Pütz, O. Daly, C.G. Morrison, M. Dunning, J.V. Kilmartin, and F. Gergely. 2013. Loss of centrioles causes chromosomal instability in vertebrate somatic cells. *J. Cell Biol.* 203:747–756. http://dx.doi.org/10.1083/jcb.201309038

Strnad, P., S. Leidel, T. Vinogradova, U. Euteneuer, A. Khodjakov, and P. Gönczy. 2007. Regulated HsSAS-6 levels ensure formation of a single procentriole per centriole during the centrosome duplication cycle. *Dev. Cell.* 13:203–213. http://dx.doi.org/10.1016/j.devcel.2007.07.004

Suh, M.R., J.W. Han, Y.R. No, and J. Lee. 2002. Transient concentration of a γ-tubulin-related protein with a pericentrin-related protein in the formation of basal bodies and flagella during the differentiation of *Naegleria gruberi*. *Cell Motil. Cytoskeleton.* 52:66–81. http://dx.doi.org/10.1002/cm.10033

Szollosi, D., P. Calarco, and R.P. Donahue. 1972. Absence of centrioles in the first and second meiotic spindles of mouse oocytes. *J. Cell Sci.* 11:521–541.

Szöllosi, D., and J.P. Ozil. 1991. De novo formation of centrioles in parthenogenetically activated, diploidized rabbit embryos. *Biol. Cell.* 72:61–66. http://dx.doi.org/10.1016/0248-4900(91)90079-3

Tang, C.J., R.H. Fu, K.S. Wu, W.B. Hsu, and T.K. Tang. 2009. CPAP is a cell-cycle regulated protein that controls centriole length. *Nat. Cell Biol.* 11:825–831. http://dx.doi.org/10.1038/ncb1889

Tang, C.J.C., S.Y. Lin, W.B. Hsu, Y.N. Lin, C.T. Wu, Y.C. Lin, C.W. Chang, K.S. Wu, and T.K. Tang. 2011. The human microcephaly protein STIL interacts with CPAP and is required for procentriole formation. *EMBO J.* 30:4790–4804. http://dx.doi.org/10.1038/emboj.2011.378

Thompson, S.L., and D.A. Compton. 2010. Proliferation of aneuploid human cells is limited by a p53-dependent mechanism. *J. Cell Biol.* 188:369–381. http://dx.doi.org/10.1083/jcb.200905057

Tiscornia, G., O. Singer, M. Ikawa, and I.M. Verma. 2003. A general method for gene knockdown in mice by using lentiviral vectors expressing small interfering RNA. *Proc. Natl. Acad. Sci. USA.* 100:1844–1848. http://dx.doi.org/10.1073/pnas.0437912100

Tsou, M.F., and T. Stearns. 2006. Controlling centrosome number: licenses and blocks. *Curr. Opin. Cell Biol.* 18:74–78. http://dx.doi.org/10.1016/j.ceb.2005.12.008

Uetake, Y., and G. Sluder. 2010. Prolonged prometaphase blocks daughter cell proliferation despite normal completion of mitosis. *Curr. Biol.* 20:1666–1671. http://dx.doi.org/10.1016/j.cub.2010.08.018

Uetake, Y., and G. Sluder. 2012. Biomedical optical phase microscopy and nanoscopy. *In* Practical Methodology for Long-Term Recordings of Live Human Cells. Academic Press, Waltham, MA. 43–52.

Uetake, Y., J. Loncarek, J.J. Nordberg, C.N. English, S. La Terra, A. Khodjakov, and G. Sluder. 2007. Cell cycle progression and de novo centriole assembly after centrosomal removal in untransformed human cells. *J. Cell Biol.* 176:173–182. http://dx.doi.org/10.1083/jcb.200607073

van Breugel, M., M. Hirono, A. Andreeva, H.A. Yanagisawa, S. Yamaguchi, Y. Nakazawa, N. Morgner, M. Petrovich, I.O. Ebong, C.V. Robinson, et al. 2011. Structures of SAS-6 suggest its organization in centrioles. *Science.* 331:1196–1199. http://dx.doi.org/10.1126/science.1199325

van Breugel, M., R. Wilcken, S.H. McLaughlin, T.J. Rutherford, and C.M. Johnson. 2014. Structure of the SAS-6 cartwheel hub from *Leishmania major*. *eLife.* 3:e01812. http://dx.doi.org/10.7554/eLife.01812

Wang, W.J., R.K. Soni, K. Uryu, and M.F. Tsou. 2011. The conversion of centrioles to centrosomes: essential coupling of duplication with segregation. *J. Cell Biol.* 193:727–739. http://dx.doi.org/10.1083/jcb.201101109

Watson, P.A., H.H. Hanauske-Abel, A. Flint, and M. Lalande. 1991. Mimosine reversibly arrests cell cycle progression at the G1–S phase border. *Cytometry.* 12:242–246. http://dx.doi.org/10.1002/cyto.990120306

Wong, Y.L., J.V. Anzola, R.L. Davis, M. Yoon, A. Motamedi, A. Kroll, C.P. Seo, J.E. Hsia, S.K. Kim, J.W. Mitchell, et al. 2015. Reversible centriole depletion with an inhibitor of Polo-like kinase 4. *Science.* 348:1155–1160. http://dx.doi.org/10.1126/science.aaa5111

Yu, J., Y. Zheng, J. Dong, S. Klusza, W.M. Deng, and D. Pan. 2010. Kibra functions as a tumor suppressor protein that regulates Hippo signaling in conjunction with Merlin and Expanded. *Dev. Cell.* 18:288–299. http://dx.doi.org/10.1016/j.devcel.2009.12.012

Lambrus et al., http://www.jcb.org/cgi/content/full/jcb.201502089/DC1



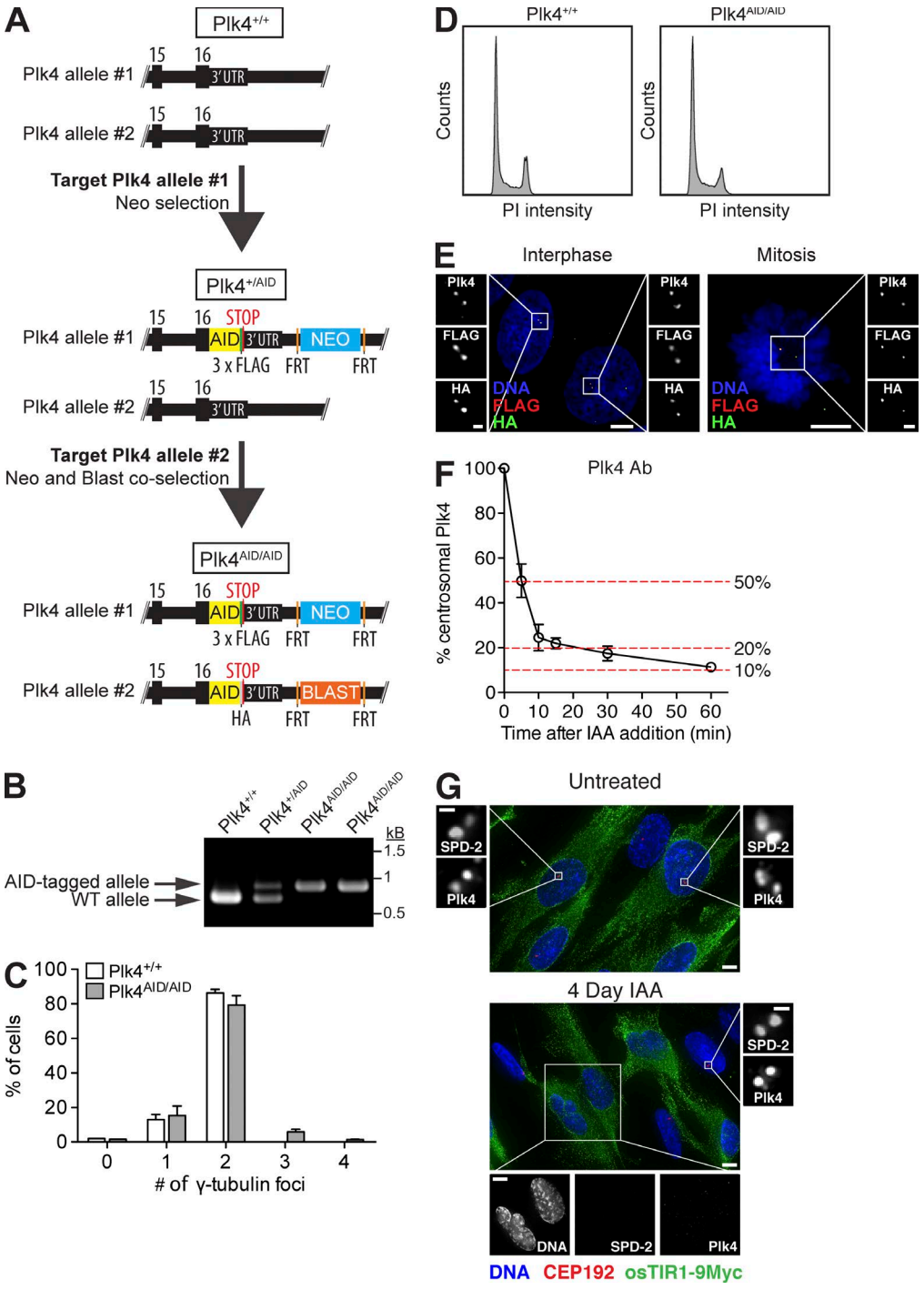


Figure S1. **Generation of Plk4$^{AID/AID}$ cells.** (A) Schematic outlining the strategy for the construction of Plk4$^{AID/AID}$ RPE1 cells. (B) Genotyping of Plk4-AID heterozygous and homozygous cells. Plk4$^{AID/AID}$ cells possess a single band corresponding to the Plk4-AID allele. (C) Quantification of the number of γ-tubulin foci in Plk4$^{+/+}$ and Plk4$^{AID/AID}$ cells. Each bar represents the mean of >100 cells from at least two independent experiments. Error bars represent the SEM. (D) Flow cytometry cell cycle analysis showing normal asynchronous cell cycle profiles for Plk4$^{+/+}$ and Plk4$^{AID/AID}$ cells. (E) Selected images of Plk4$^{AID/AID}$ cells immunostained for Plk4, FLAG, and HA. HA, FLAG, and Plk4 antibody signals colocalize in interphase and mitotic cells. (F) Quantification of the level of Plk4 at the centrosome at the indicated times after IAA addition. Each condition represents the mean of >70 cells from at least two independent experiments. Error bars represent the SEM. (G) Selected images of untreated control or IAA-treated cells immunostained with CEP192, Plk4, and Myc. 4 d after IAA addition, CEP192 and Plk4 are no longer detectable in cells expressing the F-box protein osTIR1-9Myc, but are present in neighboring cells lacking osTIR1-9Myc. Bars: (main) 5 µm; (inset) 1 µm.

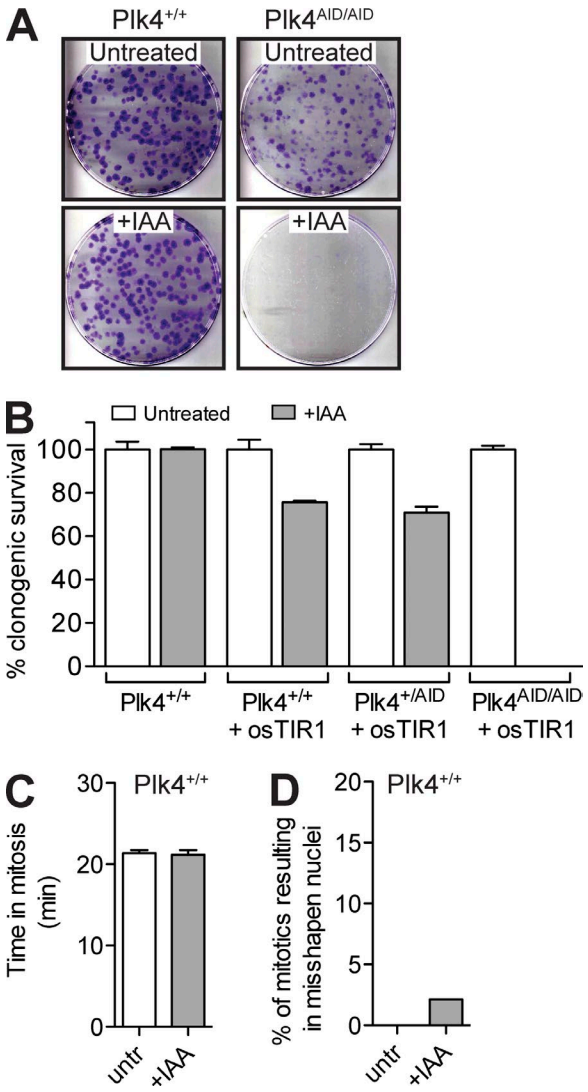


Figure S2. **Destruction of Plk4 leads to a long-term growth arrest.** (A) Representative images of crystal violet–stained colonies formed 2 wk after addition of IAA. (B) Quantification of the percentage of clonogenic survival of the indicated cell lines. Bars represent the mean of at least two independent experiments performed in triplicate. (C and D) Quantification of mitotic duration and the frequency of divisions resulting in the formation of misshapen nuclei in IAA-treated Plk4$^{+/+}$ cells. IAA has a negligible impact on mitotic fidelity. Bars represent the mean of >50 cells from two independent experiments. Error bars represent the SEM.

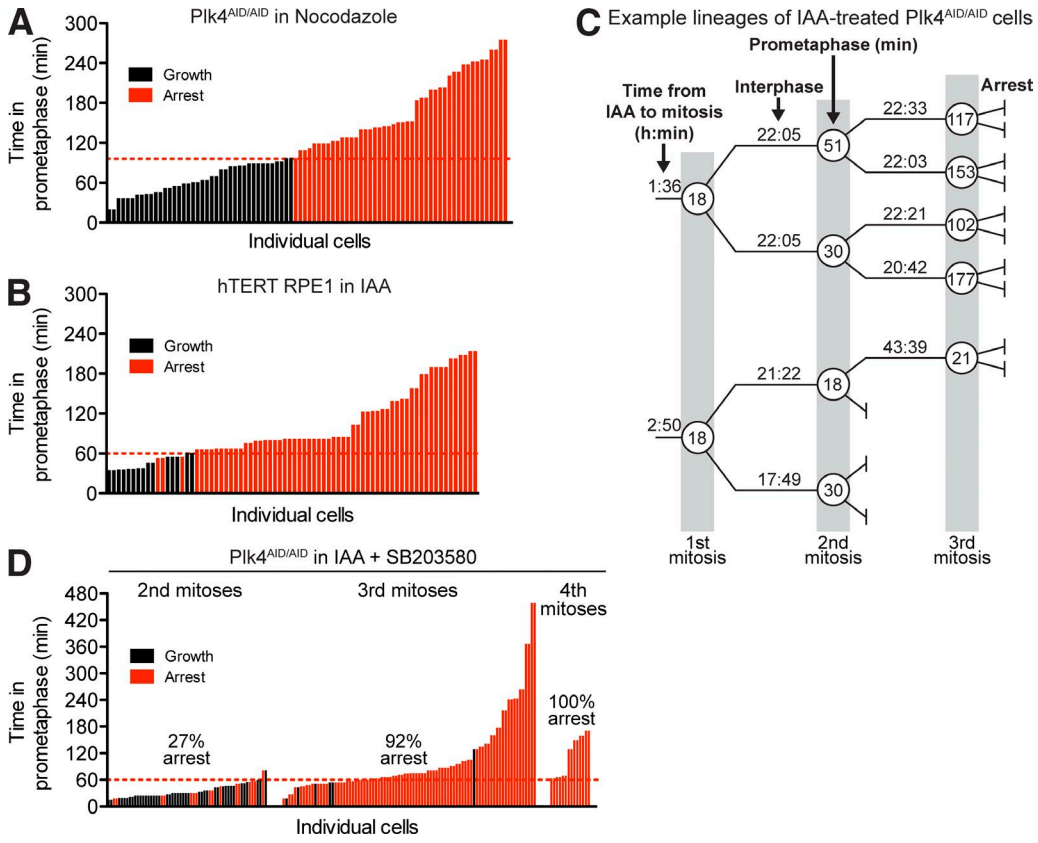


Figure S3. **Inhibiting the activity of p38 MAPK does not prevent the cell cycle arrest caused by centriole duplication failure.** (A–B) Graph showing the prometaphase duration and proliferative capacity of Plk4$^{AID/AID}$ cells or parental RPE1 cells. Each bar represents a daughter cell, its height represents the prometaphase duration of the mother cell, and its color represents the fate of the daughter. The dashed red line indicates the maximum time that cells spend in prometaphase before undergoing a cell cycle arrest. Plk4$^{AID/AID}$ cells were treated with 0.08 µM nocodazole for the first 6 h of imaging, whereas IAA was administered to parental RPE1 cells throughout the experiment. Data were acquired in a single experiment ($n$ = 87 and $n$ = 77 prometaphases, respectively). (C) Example lineages taken from the analysis presented in Fig. 4 D. Note that daughter cells can undergo symmetric or asymmetric fates. (D) Cells were analyzed as in A and B. Only cells that underwent their first mitosis within 6 h of IAA treatment were analyzed. IAA and SB203580 were administered throughout the experiment. Data were taken from two independent experiments ($n$ = 166 prometaphases).

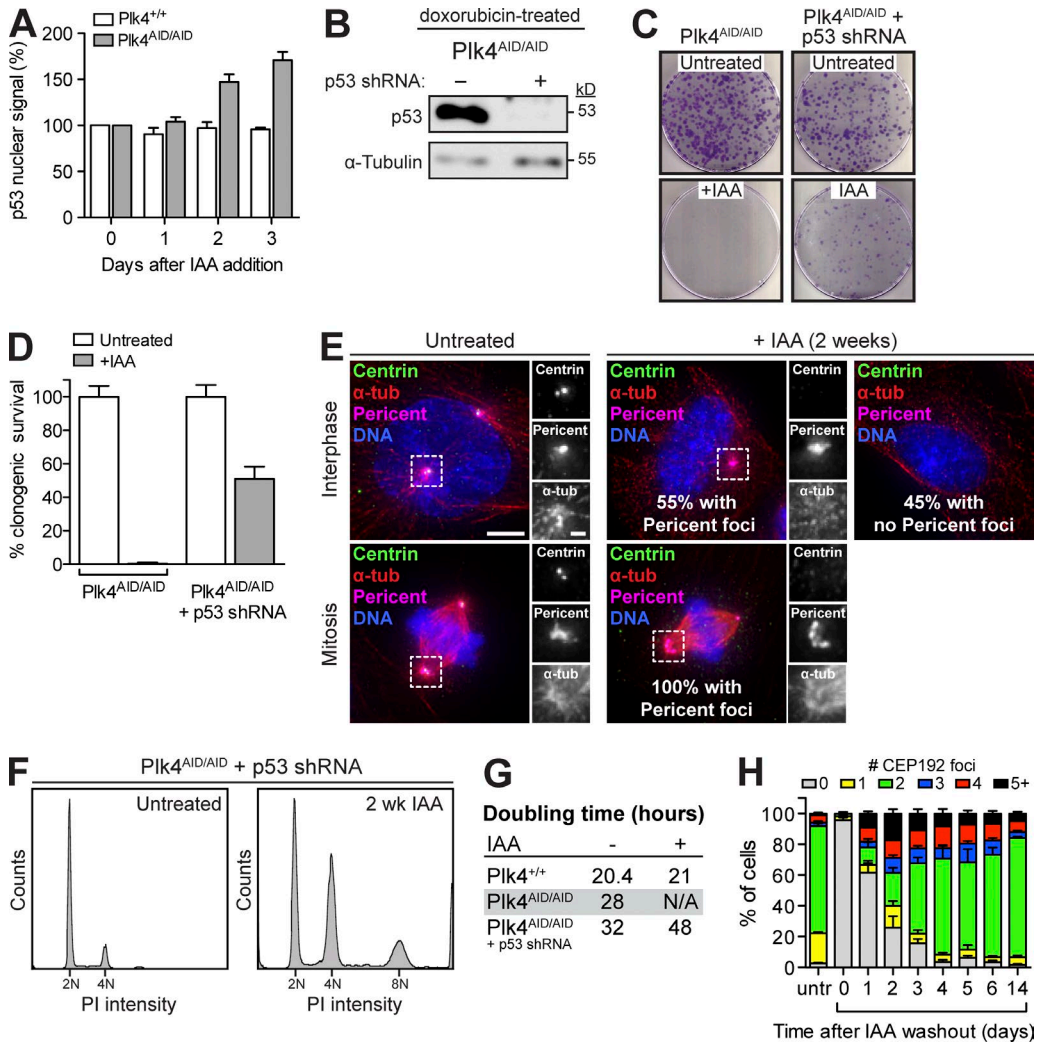


Figure S4. **Cell cycle progression and spindle assembly in the absence of centrioles.** (A) Quantification of the relative level of nuclear p53 in fixed samples at the indicated times after IAA addition. p53 levels increase after Plk4 degradation. Bars represent the mean of >200 cells from at least two independent experiments. (B) Immunoblot showing the level of p53 in doxorubicin-treated cells. (C) Representative images of crystal violet–stained colonies formed 2 wk after addition of IAA. (D) Quantification of the percentage of clonogenic survival of the indicated cell lines. p53 knockdown partly rescues the clonogenic survival of cells lacking Plk4. Bars represent the mean of at least two independent experiments performed in triplicate. All error bars in the figure represent the SEM. (E) Representative images of untreated control or acentriolar cells immunostained with α-tubulin, Pericentrin, and Centrin. Bars: (main) 5 µm; (inset) 1 µm. (F) Flow cytometry cell cycle analysis showing an increase in polyploidy in acentriolar cells. (G) Table displaying the doubling time of the indicated cell lines in the presence and absence of auxin. Doubling times were calculated from the growth curves shown in Figs. 3 A and 5 A. (H) Quantification of the number of CEP192 foci per interphase cell at indicated times after IAA washout in Plk4$^{AID/AID}$;p53 shRNA cells. Bars represent the mean of >200 cells from three independent experiments.

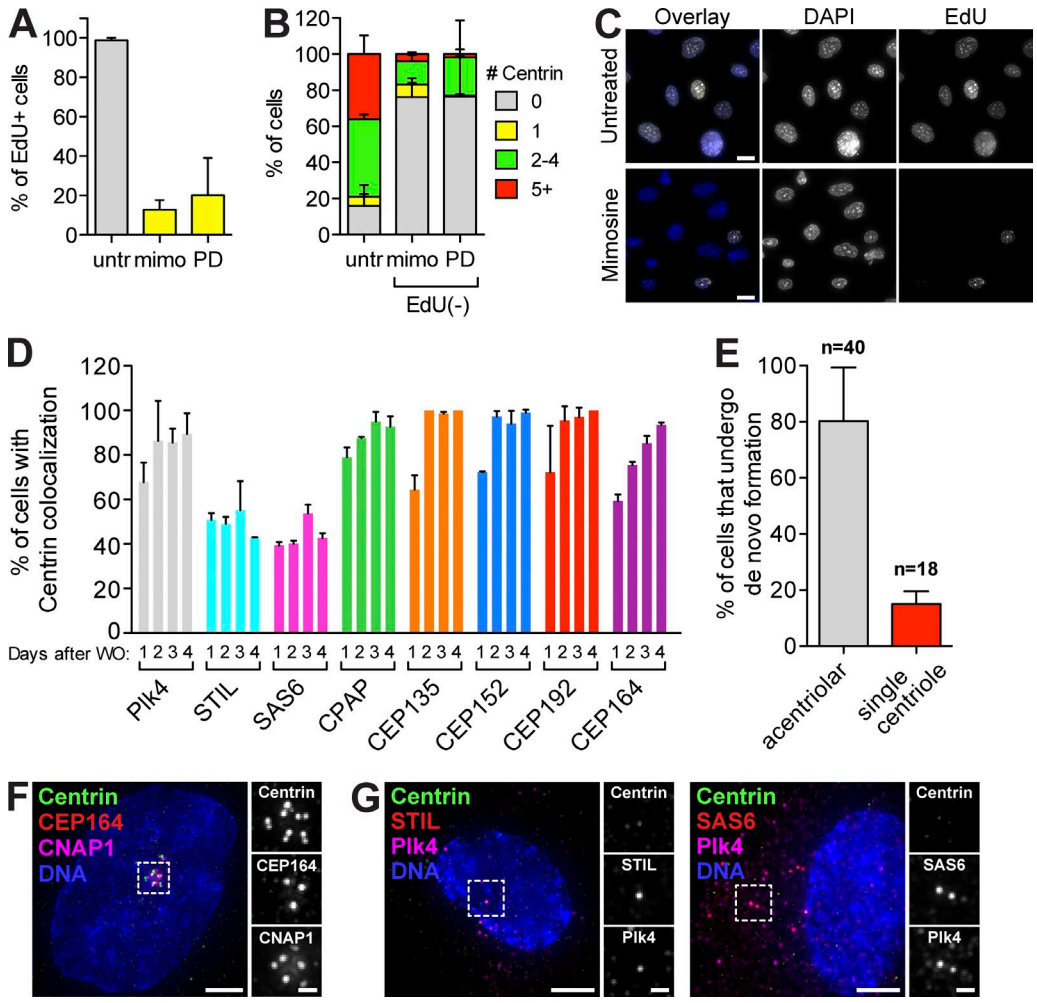


Figure S5. **De novo centriole formation requires cell cycle progression.** (A) Quantification of the fraction of EdU-positive cells. Measurements were made 2 d after release from IAA in the presence or absence of mimosine or PD0332991. Bars represent the mean of >30 cells. (B) Quantification of the fraction of Centrin foci in interphase cells. Measurements were made 2 d after release from IAA in the presence or absence of mimosine or PD0332991. Bars represent the mean of >30 cells. (C) Selected images of control untreated and mimosine-treated cells at 2 d after IAA washout. Cells were costained with DAPI and EdU. Bars, 20 µm. (D) Quantification of the fraction of interphase cells with Centrin-marked de novo centrioles that colocalize with the indicated centriole components. Quantification was derived from fixed images taken 1, 2, 3, and 4 d after IAA washout. Bars represent the mean of >40 cells from two independent experiments. (E) Quantification of the fraction of cells that underwent de novo centriole formation. Acentriolar and single centriole–containing cells expressing EGFP-Centrin were tracked for 60 h by time-lapse microscopy. Bars represent the mean of two independent experiments. All error bars in the figure represent the SEM. (F) Image of de novo centrioles 3 d after IAA washout. Cells were costained with CEP164, CNAP1, and Centrin. (G) Selected images of control de novo centrioles at 1 d after IAA washout. Cells were costained with Centrin, Plk4, and STIL. Plk4 and STIL form foci that do not colocalize with Centrin and likely represent sites of nascent de novo centriole formation. Bars: (main) 5 µm; (inset) 1 µm.

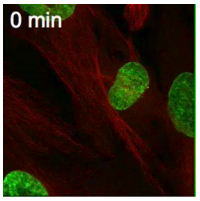


Video 1. **Movie of untreated Plk4$^{AID/AID}$ cell coexpressing TagRFP-tubulin (red), EGFP-Histone H2B (green), and EGFP-Cep63 (green).** Images were analyzed by time-lapse confocal microscopy using a laser-scanning confocal microscope. Shown in Fig. 3 G (Untreated). One frame captured every 3 min; displayed at 10 frames/s.

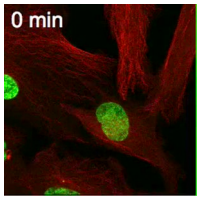


Video 2. **Movie of Plk4$^{AID/AID}$ cell treated for 2 d with IAA and coexpressing TagRFP-tubulin (red), EGFP-Histone H2B (green), and EGFP-Cep63 (green).** Images were analyzed by time-lapse confocal microscopy using a laser-scanning confocal microscope. Shown in Fig. 3 G (2 days IAA). One frame captured every 3 min; displayed at 10 frames/s.

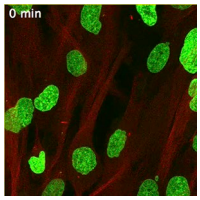


Video 3. **Movie of untreated Plk4$^{AID/AID}$;p53 shRNA cell coexpressing TagRFP-tubulin (red), EGFP-Histone H2B (green), and EGFP-Cep63 (green).** Images were analyzed by time-lapse confocal microscopy using a laser-scanning confocal microscope. Shown in Fig. 5 E (Untreated). One frame captured every 3 min; displayed at 10 frames/s.

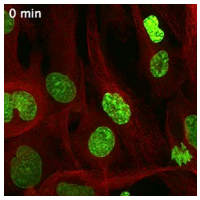


Video 4. **Movie of Plk4$^{AID/AID}$;p53 shRNA cell treated for 2 wk with IAA and coexpressing TagRFP-tubulin (red), EGFP-Histone H2B (green), and EGFP-Cep63 (green).** Images were analyzed by time-lapse confocal microscopy using a laser-scanning confocal microscope. Shown in Fig. 5 E (Chronic IAA). One frame captured every 3 min; displayed at 10 frames/s.

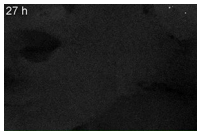


Video 5. **Movie of an acentriolar Plk4$^{AID/AID}$;p53 shRNA cell expressing EGFP-Centrin.** IAA was washed out at 0 h to allow Plk4 recovery and de novo centriole formation. Images were analyzed by time-lapse confocal microscopy using a laser-scanning confocal microscope. Shown in Fig. 8 A (Cell 1). One frame captured every 10 min; displayed at 10 frames/s.

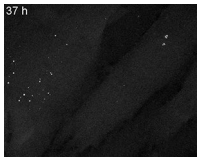


Video 6. **Movie of an acentriolar Plk4$^{AID/AID}$;p53 shRNA cell expressing EGFP-Centrin.** IAA was washed out at 0 h to allow Plk4 recovery and de novo centriole formation. Images were analyzed by time-lapse confocal microscopy using a laser-scanning confocal microscope. Shown in Fig. 8 A (Cell 2). One frame captured every 10 min; displayed at 10 frames/s.